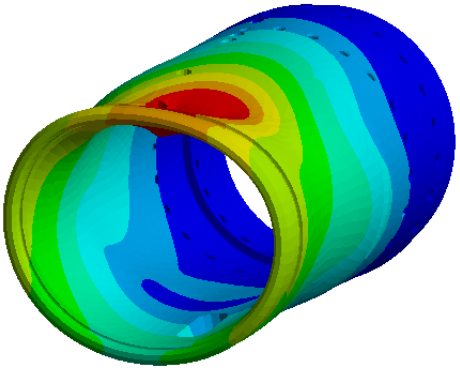

Improving turning precision of a lens barrel

Application of finite element method and mechanical analysis

ARVID ELM
FINN PRANTER

Department of Mechanics and Maritime Sciences

Chalmers University of Technology
Gothenburg, Sweden
2026

www.chalmers.se

KANDIDATARBETE 2026

Improving turning precision of a lens barrel

MMSX25

ARVID ELM
FINN PRANTER

CHALMERS

Department of Mechanics and Maritime Sciences
CHALMERS UNIVERSITY OF TECHNOLOGY
Göteborg 2026

Improving turning precision of a lens barrel

Arvid Elm
Finn Pranter

Supervisor: Erik Hagman, Dr. -ing Kristof Bandau

Examiner: Zhiyuan Li, Senior Researcher, Marine Technology, Mechanics and Maritime Sciences

Bachelor thesis 2026
Department of Mechanics and Maritime Sciences
Chalmers University of Technology
SE-412 96 Göteborg
Telephone +46 31 772 1000

Typeset in LaTeX
Cover page image: Deformed objective lens barrel captured in ANSYS
Gothenburg 2026

Improving turning precision of a lens barrel
ARVID ELM, FINN PRANTER
Department of Mechanics and Maritime Sciences
Chalmers University of Technology

Abstract

Lens barrels for optical components require high precision manufacturing for achieving acceptable form and precision. The Thorlabs production facility in Mölndal has experienced problems with unwanted deformations in microscope lens barrels. This thesis investigated the source of these deformations and connected the issue to workpiece fixturing during turning operations. Alternative concepts for workpiece holding were researched and evaluated using finite element analysis, mechanical calculation and experimental validation.

A finite element model of the current workpiece fixture was developed from solid CAD models in ANSYS 2024 R2. The model was compared to measurements of the current barrel and fixture from a coordinate measuring machine. The simulation was iterated in several steps and the final model achieved good agreement with measured data and reproduced the modes of deformation experienced in production.

Design requirements for new solutions were formulated. A number of alternative solutions were then investigated. These included a three-jaw chuck, a fixture with a clamp with relief cuts, commercial elastic collets, a shrink fit assembly and an axially compressing clamp. The concepts were evaluated based on deformation, ability to resist slipping, manufacturability and operational practicability.

Of the investigated concepts, the axial clamping fixture was assessed as the best solution due to its low predicted deformation, despite the use of conservative assumptions. The axial clamp was further refined for manufacurability and use with the machine interface.

The work demonstrates that finite element simulation, combined with experimental validation and physical measurement, can be used to analyze and improve fixturing systems for manufacturing optical components.

Acknowledgments

We want to express our gratitude to Erik Hagman and Kristof Bandau for their valuable support throughout the project. Additionally, we want to thank the entire team at Thorlabs, Nasu and Thelma for their welcoming attitude and support.

Glossary

Below is a list of words and acronyms used throughout the thesis

Ansys	Commercial software used for finite element analysis
Solidworks	Commercial software for CAD modelling
Barrel	A component that houses a lens package
CMM	Coordinate measuring machine
FEA	Finite element analysis
FEM	Finite element method
GDT	Geometric and dimensional tolerances
TL15X and LMUL	A type of microscope objective with a lens barrel produced by Thorlabs

Contents

List of Figures

List of Tables

1 introduction

Modern optical systems require extremely high geometric precision to ensure alignment and optical performance. There are several common causes of error in optical systems (Lin & Cheng, 2011). Lens barrels, the mounting house for lenses in microscopes and telescopes etc., are for instance sensitive to variations in cylindricity and concentricity between inner and outer surfaces. Minimizing these errors is crucial for reaching optimal performance of a complete system. High performance optics are used in several fields, such as microscopy on a cellular level and evaluation of circuit boards. High performance optics can also aid in the development of other modern technologies, such as lasers and satellites.

To achieve the necessary precision, the manufacturing methods must be ultra precise as well. The technologies used in ultra precision machining have been thoroughly studied (Liebrich, 2024). Conventional machining methods, such as turning, milling and grinding are central in ultra precision manufacturing. The differences between ultra-precision and conventional machining include an increased accuracy in control, vibration dampening and positioning. The ultra-precise methods can generally produce parts and surfaces with tolerances on or below micron scale. That is on a level of $10^{-6}m$.

In ultra-precision machining, the requirements for geometrical tolerances and surface quality can be very strict. Micrometer-scale deviations introduced during machining may significantly affect the results. Like regular machining, workpiece holding is a necessary step in the production of the part. In ultra-precision machining, vacuum chucks are common due to their ability to dampen vibrations and holding workpieces without distortions. The atmospheric pressure exerts a force on the workpiece and holds it against the chuck. Vacuum chucks, however, requires flat workpieces with sufficient area. Thin walled cylinders, such as lens barrels for optics can not be used with vacuum chucks and must rely on separate holding fixtures. One important source of deviations can be directly linked to the workpiece holding fixture. Elimination of fixture-induced deformations in the lens barrel is therefore a crucial aspect when ensuring a high precision finished product.

1.1 Background

Thorlabs is an international company in the photonics and optics field, with a Swedish branch in Mölndal. The components for finished goods comes from external suppliers or are manu-

factured in house by turning. The turning machine at the Mölndal facility is an ultra-precision diamond turning unit with integrated optical sensors for centering of mounted lenses. This machine is used both for optical and purely mechanical components. A common solution in optical systems is to have a sliding, cylindrical lens package in a cylindrical barrel as seen in Figure 1.

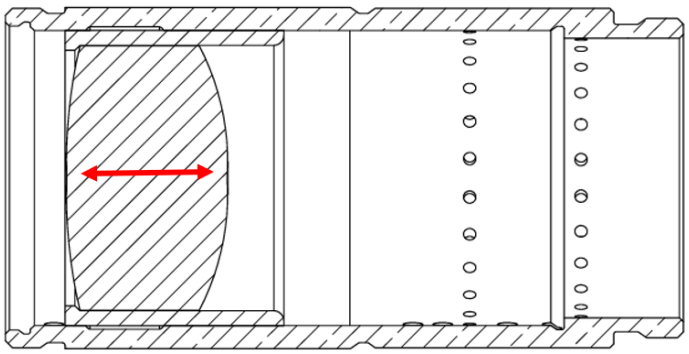

Figure 1: Concept view of a lens cell in the lens barrel. The red arrow indicates translation direction.

In order to achieve the optimal optical performance, these cylinders need to be coaxial and have a high degree of roundness. One area of improvement at Thorlabs is to further increase precision of the components that are fitted in the same optical system. As of now, the fixture used to mount the barrel in the turning machine introduces uneven stresses, which causes the barrel to fall out of specification. The current fixture uses an internal thread and an external clamp to fix the barrel. The clamp consists of an M4 screw in the upper part of the fixture, as seen in Figure 2 and Figure 3.

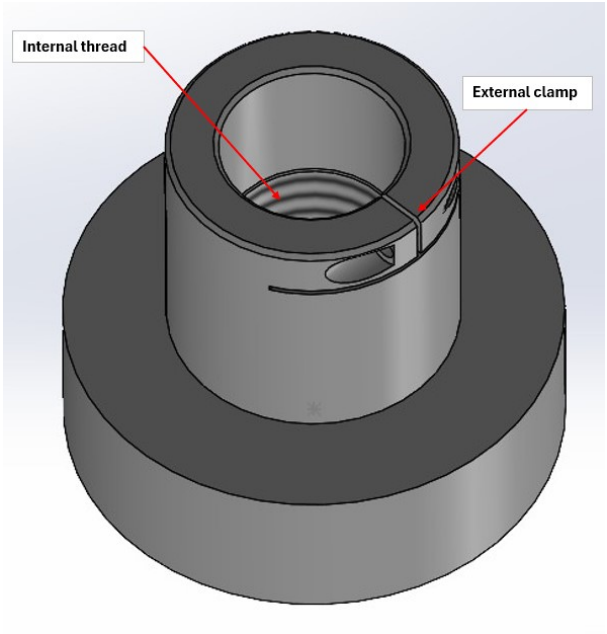

Figure 2: The current turning fixture with an internal thread and external clamp

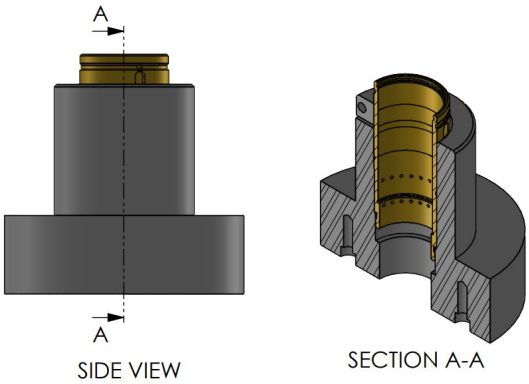

Figure 3: Side and sectional view of the barrel mounted in the fixture.

1.2 Aim

The aim of the project is to improve the turning precision of the TL15X lens barrel, while maintaining specifications set by the R&D department at Thorlabs. The turned lens barrel must achieve an adequate cylindricity of 5 μm. Additional objectives are minimization of mounting time and cost for the new solution.

This work aims to analyze and find the cause of unwanted deformations in machining of optical lens barrels. Additionally, how can unwanted deformation in ultra-precision turning of lens barrels be reduced while maintaining resistance against machining forces?

1.3 Limitations

- Due to time restrictions, physical testing of the final concept solution will not be conducted.
- The purpose of the simulation is to help find a solution to the manufacturing accuracy problem. The boundary conditions and features of the model will be applied with this goal in mind. Physical inaccuracy that does not affect the result will be neglected.
- Only static deformations of the barrel and fixture will be studied. Dynamic cutting forces has not resulted in any noticeable deformations during the machining at Thorlabs.
- Calculation of the cutting force is highly complex at the scale investigated. Cutting force calculations will therefore not be conducted.

2 Theory

The concepts developed and evaluated in this project were mainly based on the following theoretical approaches.

2.1 Geometric dimensioning and tolerancing

In a technical drawing, every measurement is specified with a nominal value. In production, this value cannot be reproduced exactly. A tolerance attached to a nominal value provides the producer of a part with a range of allowed values for a specific feature. For example, a steel beam can have a nominal length of 1000 mm with a tolerance of ± 0.5 mm. This allows the finished beam to have a length of anything from 999.5 mm to 1000.5 mm. In this work, geometrical tolerances are also used to compare how well a simulation model adheres to real measured values. Below, brief explanations of the tolerances used throughout this thesis are provided (Engineer Essentials LLC, 2026).

2.1.1 Circularity

Circularity describes how far a circular feature is allowed to deviate from a perfect circle. The upper and lower limit of the tolerance added to the nominal values can be thought of as the diameters of two imaginary circles that the finished circular feature must fit within, see figure 4.

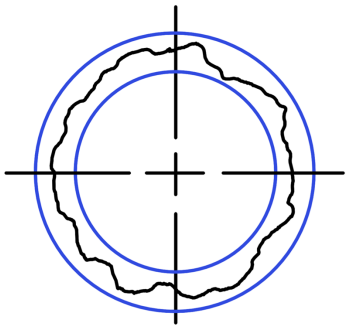

Figure 4: Circularity tolerance zone

2.1.2 Cylindricity

Like circularity, cylindricity describes how much a cylindrical feature is allowed to deviate from a perfect right circular cylinder. The finished cylindrical feature must fit between two

imaginary cylinders with radii equal to the nominal value plus the lower and upper limit of the tolerance, see figure 5.

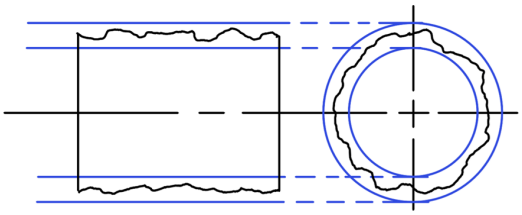

Figure 5: Cylindricity tolerance zone

2.1.3 Runout

Runout describes how much an object, when rotated around the true axis of another datum feature, is allowed to deviate with respect to that datum. Runout is measured on a 2D plane at specific heights along a feature and can therefore be imagined as the tolerable deviation from a perfect circle, concentric with the datum feature. Runout is illustrated in figure 6.

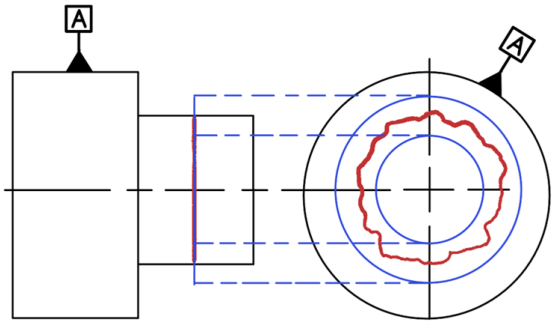

Figure 6: Runout tolerance zone

2.1.4 Flatness

Flatness specifies the allowed height distance from the lowest part of a surface to the highest part of that same surface. The difference between the upper and lower limits describes the distance between two parallel planes that the surface must fall within, see figure 7.

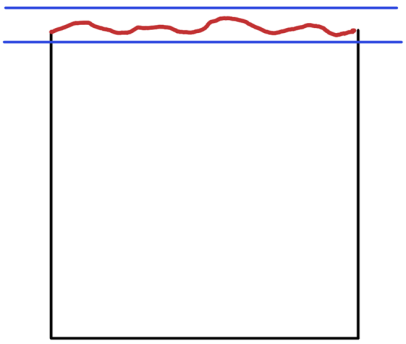

Figure 7: Flatness tolerance zone

2.2 Geometrical tolerances in optical systems

The performance of optical system is not just limited by the purely optical components, such as lenses and mirrors. The mechanical components, such as lens barrels, lens cells and spacers are also crucial in the systems since they control position and tilt of optical surfaces. The effect and magnitude of mechanical tolerances are described and exemplified by Chang and Lin (Lin & Cheng, 2011). Some major assembly variations for lens barrels are caused by poor cylindricity on the inner surface and deficient concentricity between outer and inner surfaces. These precision flaws are therefore of greatest interest when investigating the machining errors of lens barrels. The consequence of tolerance errors have further implications as well (Yoder, 2008). Avoiding tolerance errors in key components positively affects production time, inspection time and the overall total life cycle cost.

2.3 Finite Element Method

The Finite Element Method (FEM) is a widely used numerical method for solving partial differential equations that arise in engineering and physics. It can be applied to problems in basically all engineering fields, from solid and fluid mechanics to thermodynamics. It works by discretizing a continuous domain into a finite number of small elements and approximating the

field variables within each element using interpolation functions. This process transforms the governing differential equations into a system of algebraic equations that can be solved after applying appropriate boundary conditions. FEM provides approximate numerical solutions to problems where analytical solutions are difficult or impossible to obtain.

The practical application of FEM is commonly referred to as Finite Element Analysis (FEA). This analysis is usually performed with a software, such as Abaqus, Ansys or Comsol. The usage of FEA during the design and iteration process when improving or developing a new product can significantly decrease the time from idea to finished product (Kurowski, 2004). Traditionally, the design process has been iterative and time consuming, with time spent prototyping and testing models of new concepts. With FEA, the testing can be done using a digital CAD-model, thus eliminating several steps in the process. With a finalized concept that has been verified in the simulation, a physical prototype can be ordered with a higher likelihood of adequate functionality. This project will utilize FEM and FEA, but the method will not be explained in more detail. For more information on the FEM formulation, please refer to literature such as Kurowski (Kurowski, 2004).

Convergence analysis is another important part of FEM. When convergence is reached, the approximate FEM-solution to the physical problem no longer changes significantly with changing mesh size. Convergence can thus ensure numerical stability and accurate results.

In this project, all FEM simulations will be run in Ansys 2024 R2. The FEM-model will also utilize a linear elastic, isotropic material model using small deformation theory.

2.4 Workpiece holding

Workpiece holding in ultra precision machining is commonly achieved by a vacuum chuck, where atmospheric pressure holds the workpiece against the spindle. This can be done on the Thorlabs machine as well. The advantages and requisites for a vacuum chuck have previously been defined (Liebrich, 2024). One requirement for vacuum clamping is sufficient surface area and flatness. Due to the limited surface area of the investigated part, a thin-walled cylinder for optics, vacuum clamping is not suitable. Instead, workpiece holding must be attained through other methods.

Holding, or clamping, of parts with rotational symmetry is mostly accomplished by different

types of chucks and collets (Möhring et al., 2025). This report also highlights the common need for specific designs for workpiece holding in ultra high precision machining and the lack of standard solutions for thin walled parts. Machining of thin walled cylinders and clamping optimizations by FEM have also been previously studied (Patalas et al., 2018).

2.5 Cutting forces

A literature study regarding cutting forces was also conducted, as the workpiece holding demands are constrained by the forces exerted on the part. Cutting force calculations are rigorously explained in literature (AB Sandvik Coromant, 2021). The theories available are however focused on conventional machining without a clear connection to ultra high precision machining. In ultra high precision machining, force determination is highly complex due to new phenomena such as plowing and squeezing (Wang et al., 2021). These methods were assessed to be outside the scope of the project.

2.6 Smoothing of noisy data

Measured data from an imperfect reality has to be treated. A filtering function in Python can address this challenge. The filtering function used was savgol_filter from the *scipy.signal* library. This function utilizes the Savitzky Golay smoothing filter, widely used in signal processing applications (Gallagher, 2020). This filter smooths functions by optimizing low degree polynomials to sub sets of the data, using the method of linear least squares. This keeps the global features, such as peaks and valleys, but removes the noise. The arguments for the function are window size and polynomial degree. The window size controls the number of data points used for the polynomial fit and the polynomial degree decides the order of the polynomial used for the approximation of the functions shape without the noise. A window size of 11 and polynomial degree of 2 was used in the project.

3 Methodology

The work consisted of several clearly separate sections. The first step was to create a simulation that realistically mimicked the current problem of deformation in the lens barrel. A realistic simulation was important, partly to verify the source of the machining inaccuracy and partly to establish a method of modeling where the knowledge gained could assist in further simulation tests of alternative solutions.

Secondly , the demands from machining, such as the torque the fixture was required to resist, needed to be defined and understood to be able to determine the design criteria of a solution for improved turning precision. With the issues from the current solutions mapped, in combination with other demands from Thorlabs, the requirements for a new solution were known.

The third step was to find or develop a group of solutions that could prevent uneven stresses in the workpiece. Suggestions for an improved solution were gathered from market surveys and previous academic work. A variety of possible concepts helped facilitate a design choice process where dissmissal or acceptance of solutions were continuously made based on previously defined criteria. This step can generate good solutions, but also dismiss poor ones. The dismissal of poor solutions was also important, since it could aid in future challenges with turning precision.

The last step was to finalize the design of a chosen concept. Verification of the selected concept was done either by simulation or calculations.

3.1 Analysis and simulation of deformations

To realistically recreate the conditions that cause the barrel to deform, accurate measurements and simulations were necessary. The measurements were used both to understand the real deformations and as verification data for the simulations. A mathematical model run in Python was used to evaluate how well the simulated deformation data adhered to the measured data.

3.1.1 Physical measurement of the lens barrel

A physical measurement of the barrel using a Coordinate Measuring Machine (CMM) was conducted. The CMM uses a probe to capture the coordinates of the points on the part surfaces, shown in figure 9. The machine is able to measure both dimensions and form tolerances at a

micrometer level. The result from the CMM is therefore the most accurate depiction of the actual form of the part available in the project. For this particular case, measurements of the maximum and minimum diameters, along with a roundness and runout value, were evaluated at several heights. The heights were primarily chosen between holes and slots in the barrel to prevent the data from being polluted by these surface features. The positions of the measuring heights are presented in figure 8. The exception was height 1, which was chosen for its position in the center of the clamp. The tensioning load was applied at the clamp, which is why it was identified as an area of interest. The barrel was measured several times, both unclamped and with the clamp screw tightened to a known torque described in section 3.1.2. A final repeated measurement with the fixture unclamped was conducted to ensure that the barrel was not permanently deformed, which it was not.

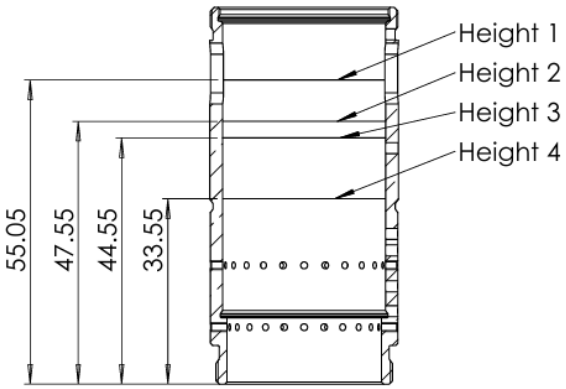

Figure 8: Measuring heights in mm for the barrel

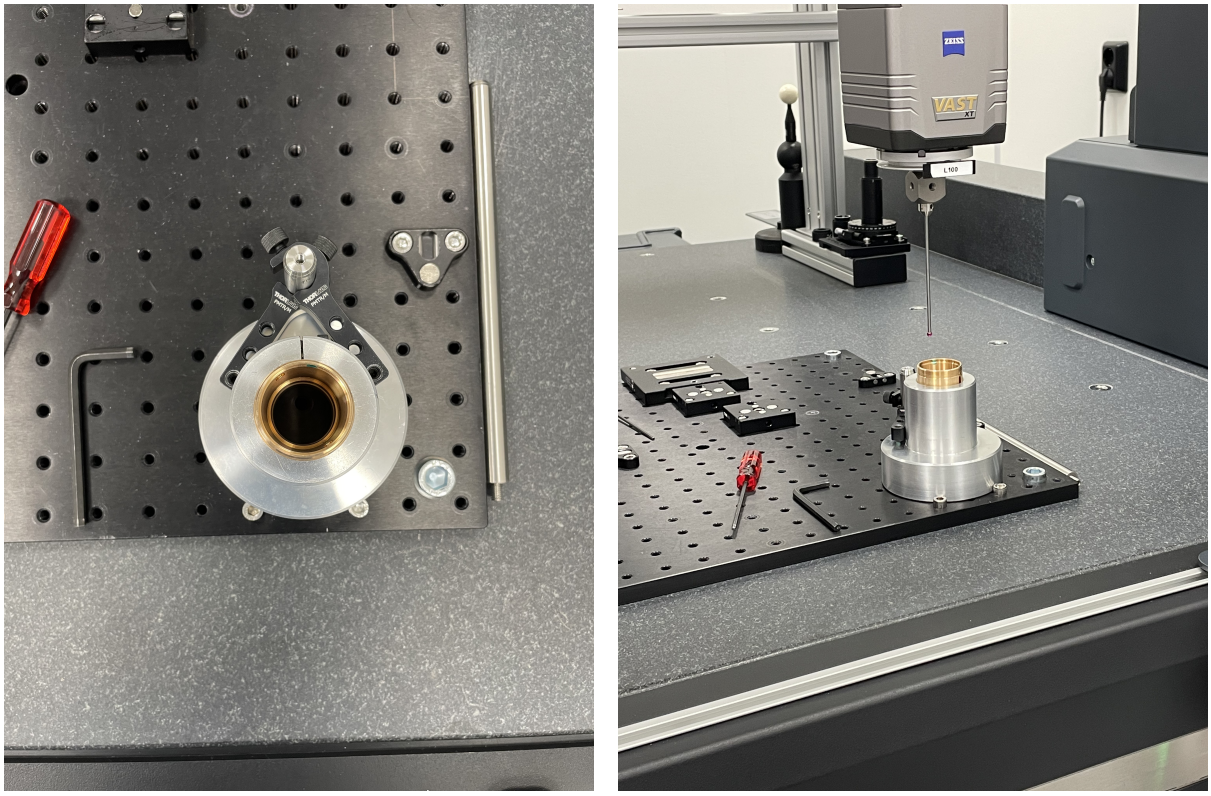

(a) measturing setup (b) Measuring process with the probe in action

Figure 9: Measuring in the coordinate measuring machine (CMM)

In the comparisons between the measured and the simulated deformations, not all datasets from the CMM were used. Measurements were taken when the fixture was tightened with a torque of 1 Nm at height 2. This value was based on clamping torque in current production. This height was chosen for its closeness to the clamp and for the fact that it was not disturbed by the slots in the barrel. The measurement values were then compared to the results of several simulation iterations. The values from the simulation were gathered from the same height as those from the CMM. An image displaying the CMM values, exaggerated with a program controlled constant, can be seen in figure 10. The blue outline shows the actual measured values and the black outline shows a reference circle. Every measurement point has a corresponding red vector arrow that, all together, almost entirely fills the space between the outlines.

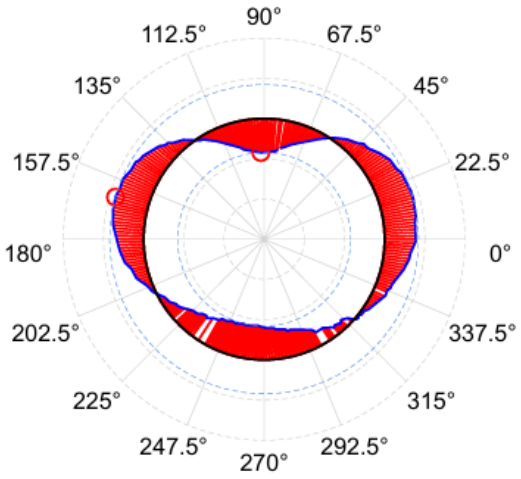

Figure 10: Plotted graph from the CMM user interface

3.1.2 Simulation setup

To replicate the measured deformation, a 3D-assembly was set up in the CAD software Solidworks. An important modification was to slightly change the internal diameter of the fixture. Initially, it had the same nominal value as the outer diameter of the barrel. After doing a CMM-measurement of the free, unclamped fixture, the actual internal diameter was changed from $34,2\,\text{mm}$ to $34,22\,\text{mm}$. The assembly was then imported to the FE-software Ansys.

In Ansys, an initial setup was prepared. This setup gave a starting point for creating a realistic simulation. It became subject to change during several iteration steps to further increase the models accuracy. The initial setup is described in this section and the iterations are described in section 3.1.5.

The model was constrained with fixed supports in the bottom screw holes, as seen in figure 11. Contact formulations were added to the internal thread in the fixture and the upper, smooth part. The thread was assumed to be ideally stationary during the whole assembly and machining process, which is why it was set to *bonded*. *Bonded* contact can neither slip, nor separate. The *Bonded* area was constrained to just a section of the thread to allow for deflection of the upper part, caused by the clamp. This section is the red part of the barrel in contact with the fixture, as seen in figure 12. The upper part of the barrel was set to *frictional* contact. This type allows for frictional sliding and separation between the parts. A researched value for friction coefficient between aluminium and brass was difficult to obtain. An approximate value of 0.4 was used as a starting value after finding researched values of aluminium to aluminium (The

Engineering ToolBox, 2004). The effect of different friction coefficients was however explored and is further discussed under section 3.1.5.

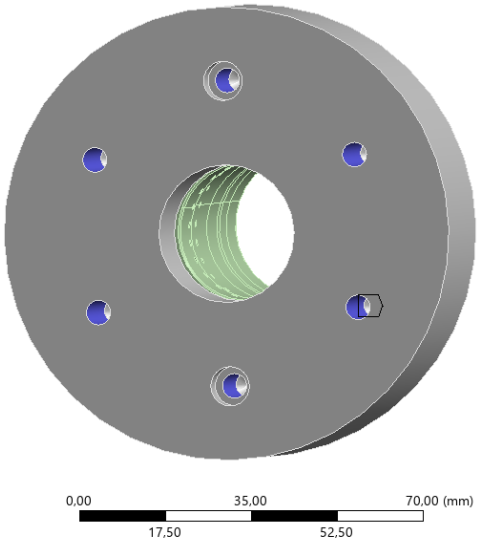

Figure 11: Fixed supports in the bottom screw holes of the fixture

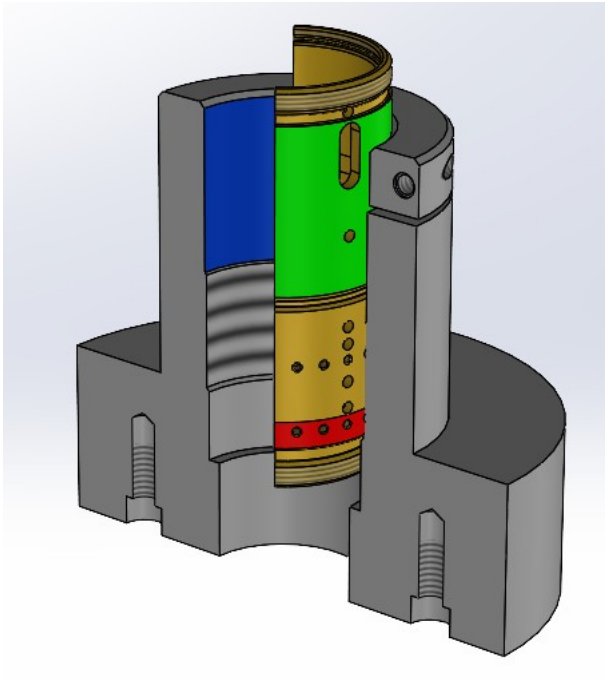

Figure 12: Section view of the fixture with mounted barrel. The red and green areas are subjected to different contact formulations

For the application of the clamping force it was necessary to translate an applied screw torque into an axial screw force. Since the screw used in the fixture was a standard ISO 4762 M4-screw, this calculation was done using the, in literature derived, equation 1 (Mägi et al., 2017).

In production, the mounting of the barrel in the fixture is currently done by angle tensioning. The screw is tightened until the head base is just in contact with the fixture. Then, the screw is rotated an additional 45-50 degrees. The angle is approximated with eye-measurement only, which makes this method unreliable. By tightening the screw 45 degrees with a torque wrench, it was determined that this tightening angle corresponded to approximately 1 Nm.

$$F_{ax} = \frac{M_{tot}}{0.16P + 0.58\mu d_2 + \mu_b r_m} \tag{1}$$

M_{tot} refers to the applied torque on the screw. P is the thread pitch, 0.7 mm for this screw. The mean diameter, d_2, is 3.545 mm and the mean radius, r_m for the screw head was 3.5 mm. The frictional coefficients were uncertain parameters in this calculation. μ_b describes the friction between the head base and μ describes friction in the thread. For unlubricated surfaces, these values can range from 0.18-0.35 (Mägi et al., 2017), making an exact value challenging to obtain. A conservative calculation with both coefficients equal to 0.18 yields the highest force and thus highest deformation in the simulation. For 1 Nm torque, the resulting axial force was between 486 N ($\mu = 0.35$) to 899 N ($\mu = 0.18$). The deformation in the barrel should therefore be the result of a force between these values. A force value between the extreme values was then added to the screw faces in Ansys, as viewed in figure 13. Forces from 490 N in incremental steps of 10 N were simulated and compared to the runout values from the second height in the CMM measurement. A force of 510 N proved to be closest to the measured result, and it was therefore chosen as starting value for further iterations, presented in table 1.

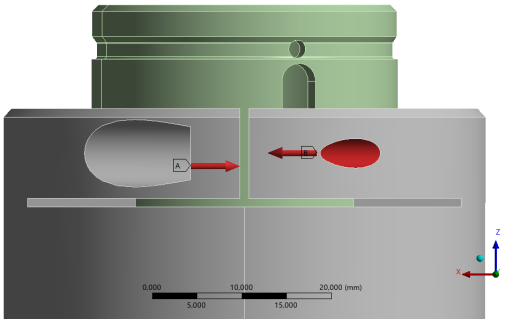

Figure 13: The applied screw forces and their directions

Due to the high precision and small deformations of the project, convergence was set to 1 percent. The mesh was automatically made finer over the contact area with the program controlled convergence tool. In order to reduce the necessary computational power, defeaturing of non-

load bearing parts was done after a first analysis. This resulted in removal of features such as chamfers and fillets.

3.1.3 Method for evaluating simulation quality

The simulation in Ansys provided between 50 and 60 measurements of the radial deformations along a circular path on the inside surface of the lens barrel, see figure 14.

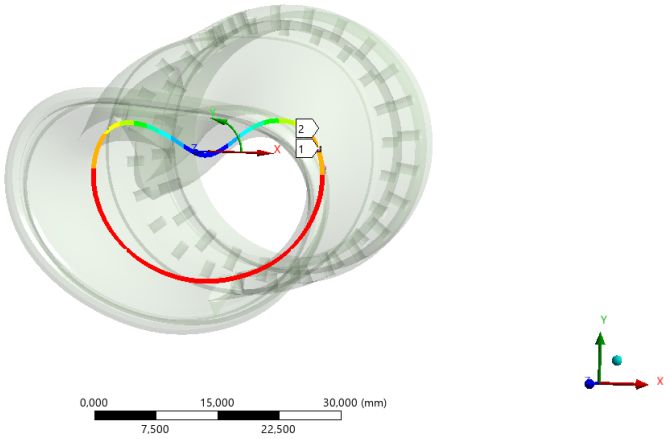

Figure 14: Circular path showing exaggerated deformation

To validate the quality of the simulation, a comparison to the measurements from the CMM was required. This comparison was made in several steps. Firstly, data was exported from both Ansys and the CMM. The data points from the circular path in Ansys was to be compared to the corresponding path from the CMM-measurement. The Ansys data was in the form of a path length and corresponding radial deformation. The CMM data had approximately 3700 coordinate-points in cartesian coordinates. A conversion of both data sets to polar coordinates was made. The datasets were imported and plotted as radius over angle in Python. The plots can be seen in figure 15 where the simulated values are represented in green and the measured values in blue.

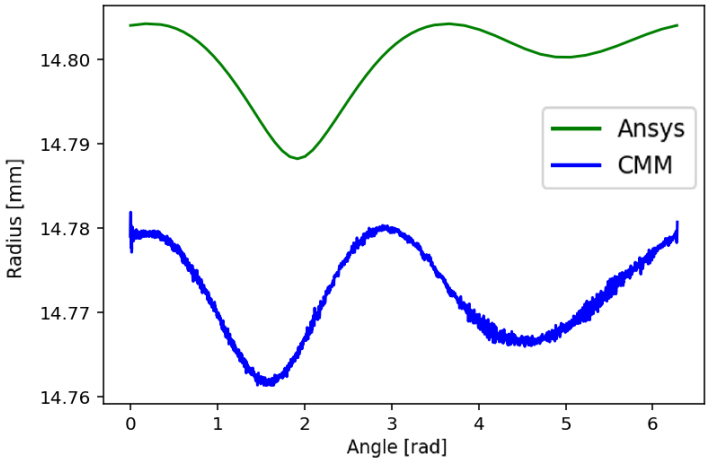

Figure 15: Comparison of CMM measurements and the first iteration of FEM simulation

The CMM-data was noisy, which would make a direct comparison to the Ansys data unreliable. The noisy data was smoothened with the savgol_filter function in python. Additionally, there was a spike in the amount of noise early in the measurement values. The greatest outliers among these values were removed manually to avoid unwanted interference with the smoothing function. The filtered function was then used for comparison. Figure 16 shows the filtered values in red compared to the original noisy values in blue.

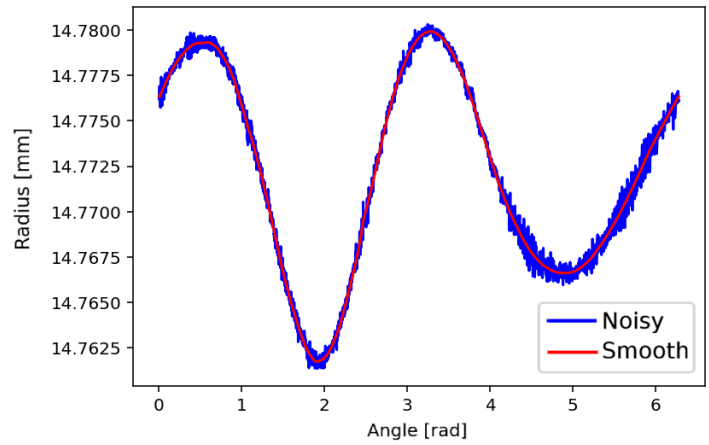

Figure 16: Smoothed function in red compared to the noisy function in blue

From the plots shown i figure 15, it was evident that the shapes were visually similar, but not in phase with each other. This would also have to be corrected before an actual comparison. The uneven pressure from the clamp caused a clear indentation, both in the CMM and the Ansys simulation, where the deformation was greater than anywhere else along the circumference. This indentation where the radius was at its smallest, was used as a reference point to align

the CMM values with the simulated values. Graphs for the Ansys and CMM data were plotted in phase as radius over angle. Figure 17 shows the simulated values in green and the phase shifted, smoothed and interpolated values from the CMM in orange. The vertical line shows the smallest radius of both plots.

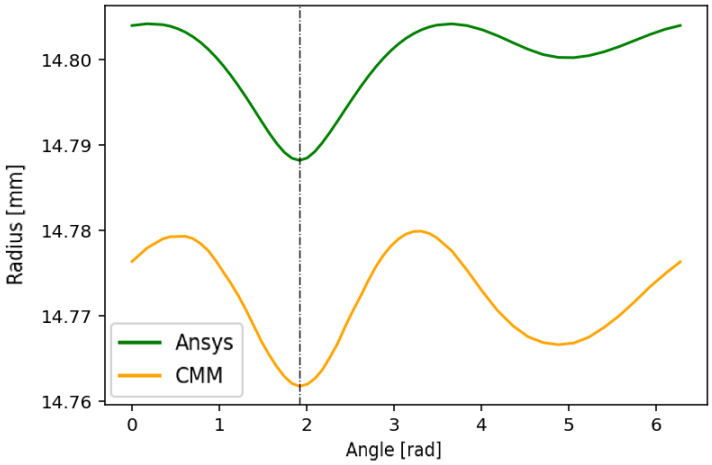

Figure 17: CMM values with angles aligned to those of the simulated values

The mean difference between the plots was used as a comparison method to evaluate the quality of the simulation.

Since the data sets still had different amounts of data points, the mean difference could not be calculated immediately. Instead, angle and radial values from the CMM dataset were linearly interpolated to the corresponding Ansys-values. This resulted in 50 to 60 data points with angles and radial values that could be directly compared. The CMM values were chosen for interpolation because they had much closer spacing and would thus give smaller errors when interpolating. Figure 18 shows an example of how a smaller data set can give a larger error using linear interpolation.

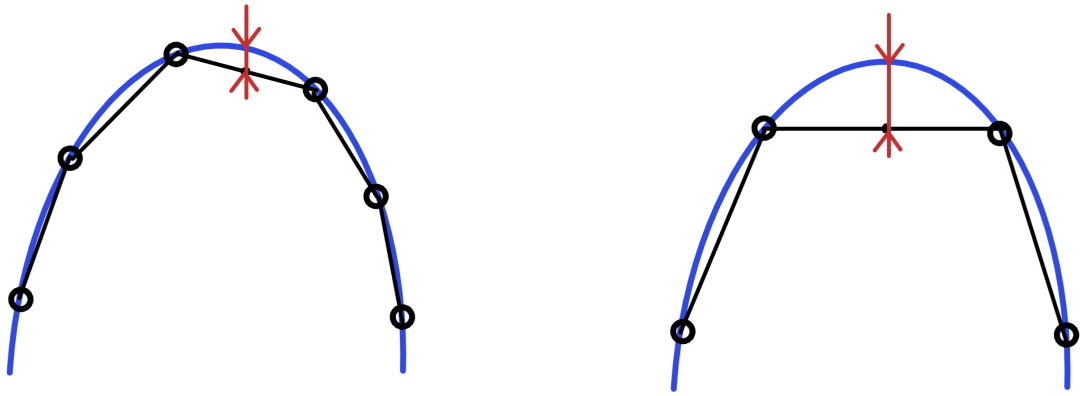

(a) Large dataset (b) Small dataset

Figure 18: The magnitudes of the errors are shown in red, where the smaller dataset clearly has a larger error

With a finished comparison model, work to further improve the simulation was initiated. This was an iterative process where inputs were changed one by one. Changes that improved the mean radial difference were kept for further iteration. Changes that worsened the mean radial difference were rejected, and new changes continued from the previous iteration. Each iteration is described in further detail under section 3.1.5.

3.1.4 Initial comparison between measurement and simulation

The deformation mode of the fixture and barrel remained largely unchanged, despite variations in parameters such as forces and friction coefficients. The initial iteration, used a 510 N force, the nominal inner barrel radius of 14.8 mm and a friction coefficient between barrel and fixture of 0.4. The resulting average difference between CMM measurements and Ansys was then 0.0267 mm. Figure 19 shows the unscaled deformation of the barrel in the fixture under the parameters in iteration 1. The effect of the asymmetric clamp is clear.

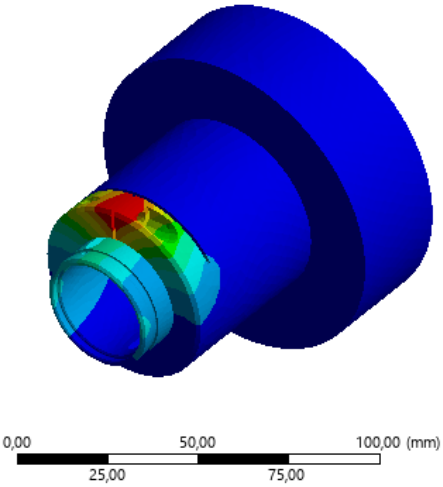

Figure 19: Unscaled deformation plot of the barrel in the fixture. The clamping part of the fixture is notably deformed, where the rest of the fixture is largely unaffected

Figure 20 shows the scaled deformation of the barrel with iteration 1 parameters.

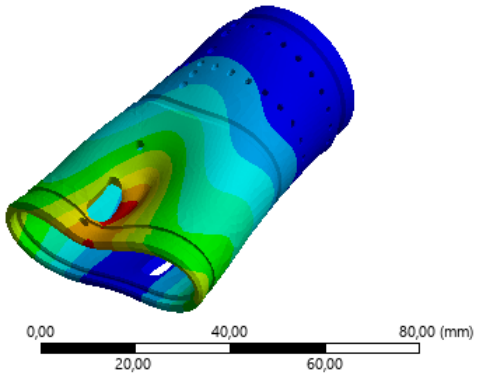

Figure 20: Scaled deformation of the barrel

Lastly, figure 21 shows plots for radial deformations at heights 2, 3 and 4. The plot for height 1 did not form a complete circle due to the slot cut in the barrel, which made this height unsuitable for comparison. The three height plots prove that deformations are greater at the top of the barrel, close to the clamp.

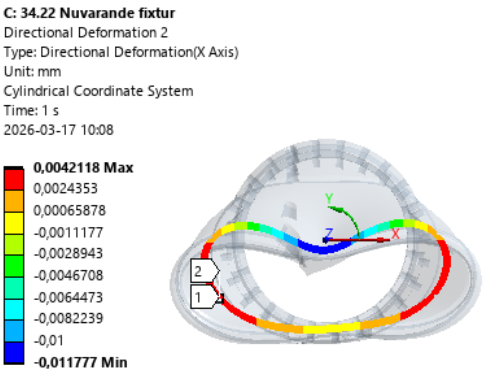

(a) Deformation at height 2

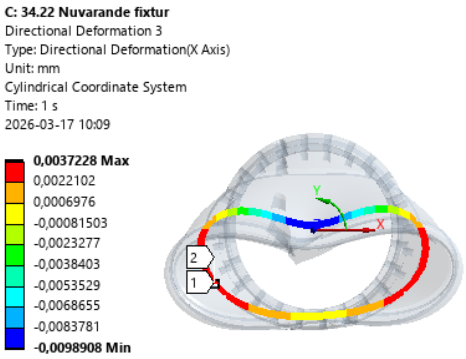

(b) Deformation at height 3

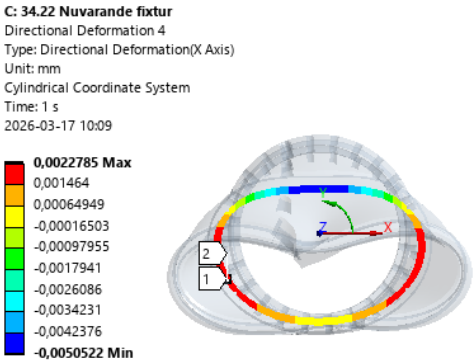

(c) Deformation at height 4

Figure 21: Differences in radial deformations at different heights

3.1.5 Iterations

The iterations consist of small changes to the initial concept described in section 3.1.2. Every iteration had somewhat different boundary conditions and contact formulations. Figure 22 shows the different contact regions that are mentioned in the iterations.

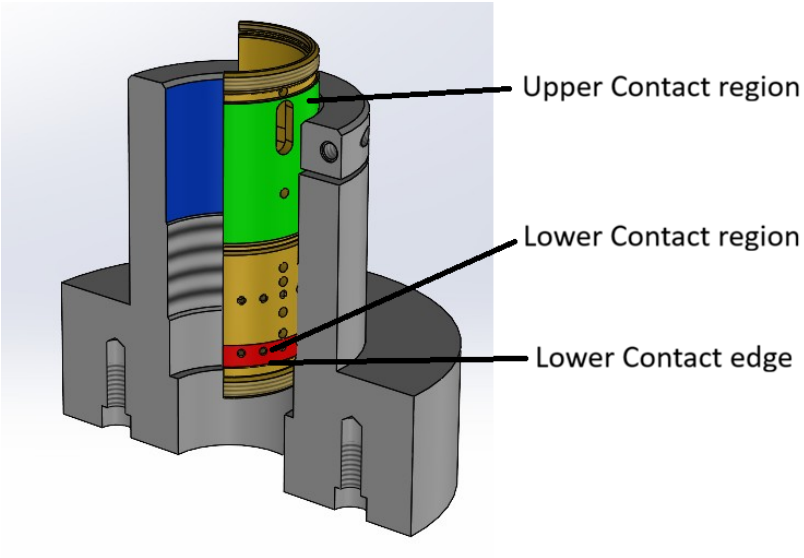

Figure 22: Contact regions

In the following, an explanation of the differing parameters in each iteration is given. Every iteration description is followed by a figure (figures 23 - 31), where the varying radii of the simulated values (green) and the measured values (orange) are plotted over the angle corresponding to each simulation value.

Iteration 1: The bottom contact region was set to bonded and the upper contact region to frictional with a friction coefficient of 0.4. The outer radius of the barrel was set to the nominal value 14.8 mm as specified in the technical drawing.

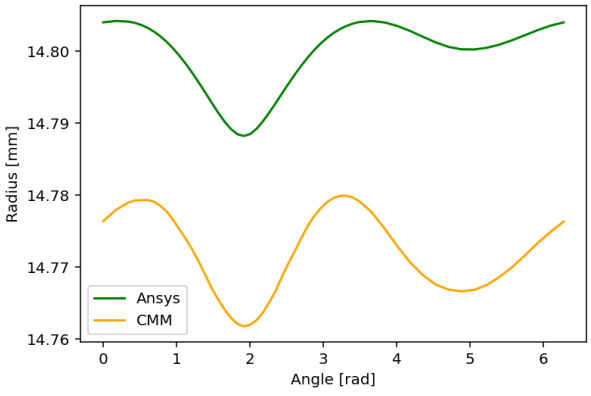

Figure 23: CMM vs. Ansys, iteration 1.

Iteration 2: The outer radius of the barrel was set to the same value as the average outer radius obtained from the CMM measurements. All contact parameters and boundary conditions remained the same as in iteration 1.

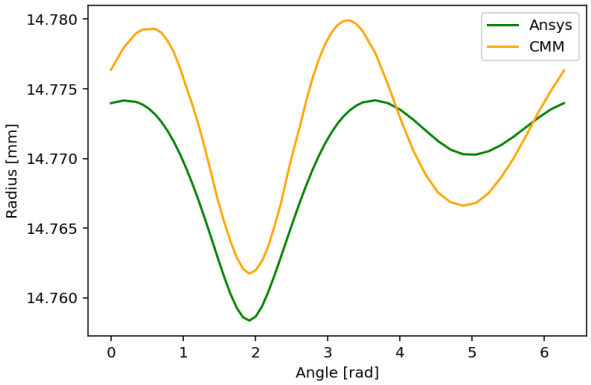

Figure 24: CMM vs. Ansys, iteration 2.

The radial values from the simulation showed closer adhesion to those from the CMM but the general shape of the deformations remained similar. As visible in table 1, this represented the single greatest improvement in average difference between simulated and measured values.

Iteration 3: Theoretically, the axial force in the clamping screw could vary over a span from about 486 N to 900 N. 510 N of axial force in the screw proved to produce the best deformation shapes according to the rounout comparison between simulated and measured values. To see if this held for the radial measurement values, a force of 600 N was applied in iteration 3. The contact formulations remained the same.

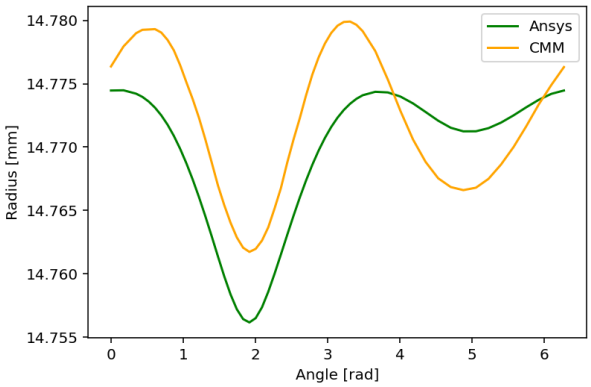

Figure 25: CMM vs. Ansys, iteration 3.

The overall deformed shape remained similar, but the average difference increased, proving that a greater force did not yield better results. The rest of the iterations were carried out with an axial screw force of 510 N.

Iteration 4: Since the coefficient of friction for brass on aluminum was not known, different values were tested. In iteration 4, the coefficient of friction was lowered to 0.2 and all other contact formulations and boundary conditions remained the same as in iteration 1, that is bonded contact for the lower contact region and an axial screw force of 510 N. Figure 26 shows that the general shape was similar to iteration 3 and 4 but the average difference was increased.

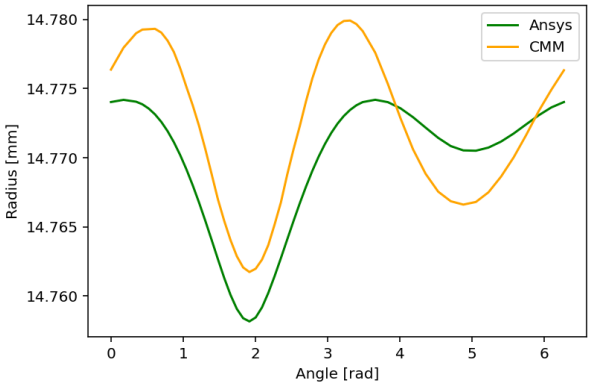

Figure 26: CMM vs. Ansys, iteration 4.

Iteration 5: The bonded lowered contact surface was thought to maybe impede realistic movement of the barrel during clamping. It is possible that the thread does not prevent the barrel from tilting in a way that results in a small gap in the threads as exemplified in figure 27.

Figure 27: Threads separating as a result of uneven clamping

To mimic the possibility of this behavior the bonded, lower contact area was removed and replaced by locking all translation and rotation of the lower edge seen in figure 22.

This resulted in an improved average difference but overall similar shape as seen in figure 28,

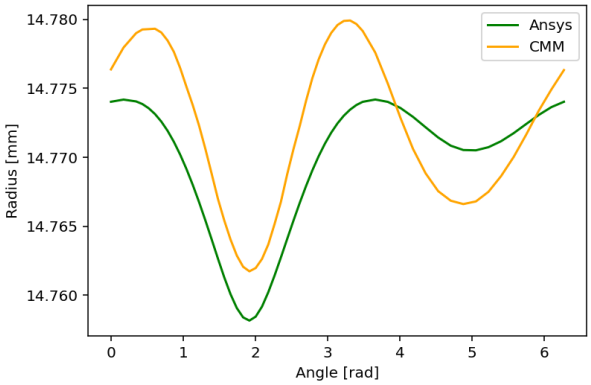

Figure 28: CMM vs. Ansys, iteration 5.

Iteration 6: From previous iterations, a small but rather constant difference between the datasets was noted. When evaluated at the first angular value, this difference was evaluated to around 0.003 mm. The CAD was updated accordingly and the simulation was processed again. The change in inner radius shifted the curve upwards, providing a better mean radius difference. The new graph is presented in figure 29.

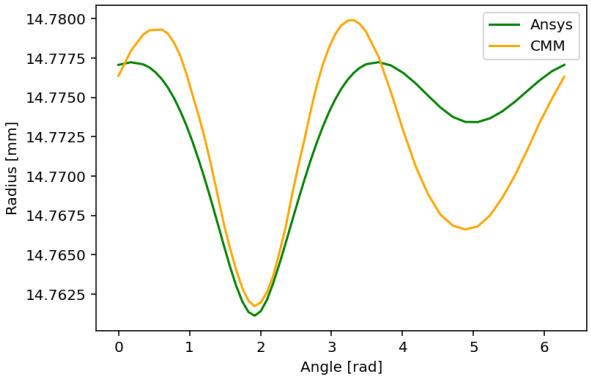

Figure 29: CMM vs. Ansys, iteration 6.

Iteration 7-9: Next, since a lowered friction had been tested, it was natural to try the other way around as well. The friction was increased in 0.2-increments for three iterations, with an improved mean radius difference for each increase as result. The friction coefficient between aluminum and brass were initially a large source of uncertainty, since experimentally obtained values were not found. The comparison between iteration 10 and CMM measurement is presented in figure 30.

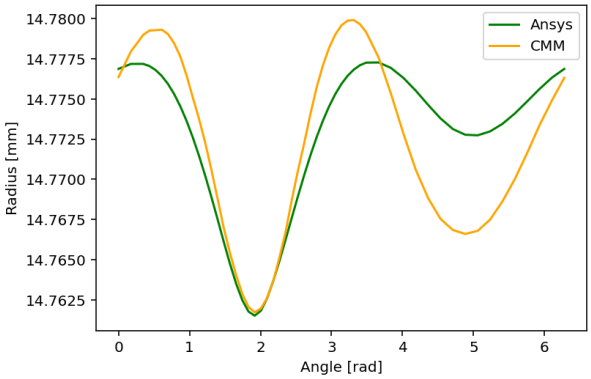

Figure 30: CMM vs. Ansys, iteration 9.

Iteration 10: A steady decrease in average difference was apparent every time the friction in the upper contact area was increased. To investigate the extreme case, the contact formulation was changed to rough, meaning that if contact is detected, no sliding is allowed (Sunar, 2021). The lower contact edge remained fixed in all 6 degrees of freedom and the force was kept at 510 N. This gave an average difference of 0.0021 mm between the simulated and measured radial values. Figure 31 shows the result of the final iteration.

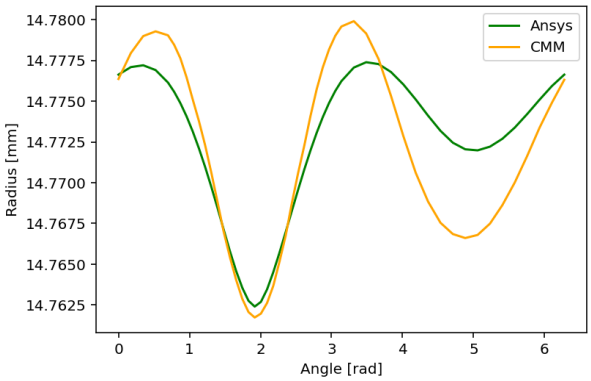

Figure 31: CMM vs. Ansys, iteration 10

The greatest deformation differs a bit more than in iterations 7 - 9 but the overall result is better.

Conclusion Table 1 shows the setup and corresponding mean average difference between the radial deformations measured in the CMM and those from the Ansys simulation.

Table 1: Iterations for simulation improvement

Iteration	Description	r barrel [mm]	Force [N]	Friction	Average difference [mm]
1	Initial	14.8	510	0.4	0.0267
2	Barrel radius decreased	14.77	510	0.4	0.0043
3	Increased force	14.77	600	0.4	0.0050
4	Decreased friction	14.77	510	0.2	0.0045
5	Bonded contact replaced	14.77	510	0.4	0.0044
6	Barrel radius increased	14.773	510	0.4	0.0029
7	Increased friction	14.773	510	0.4	0.0027
8	Increased friction	14.773	510	0.6	0.0026
9	Increased friction	14.773	510	0.8	0.0025
10	Increased friction	14.773	510	Rough	0.0021

There are several notable takeaways from the iteration round. The main cause of deformation is the fixture holding the workpiece. The diameter variation of the barrel is greatly affecting the deformation. Even the small tolerance of the diameter can be the difference between a tolerated result and failure. The surfaces are affected by relatively high forces that resist relative motion. Another important insight was that the thread will experience some play instead of being completely fixed. An uneven clamp can cause tilt that result in a slight bent shape, when examining the whole surface.

3.2 Map the demands for machining

The turning machine at Thorlabs (shown in figure 32) is capable of ultra high precision and alignment of the optical axis to the actual center of a lens package. Moreover, the unit can also be used for precision turning of purely mechanical components, such as the lens barrel in this project. Aside from some specialized solutions for higher precision, such as a granite bed and pneumatic leveling, the unit has the usual components of a turning machine. The workpiece, the objective lens barrel, is mounted using the fixture on the machine specific, pneumatic interface. The tool is mounted on a tool holder, moving in radial and axial directions. The spindle can rotate both clockwise and counter clockwise.

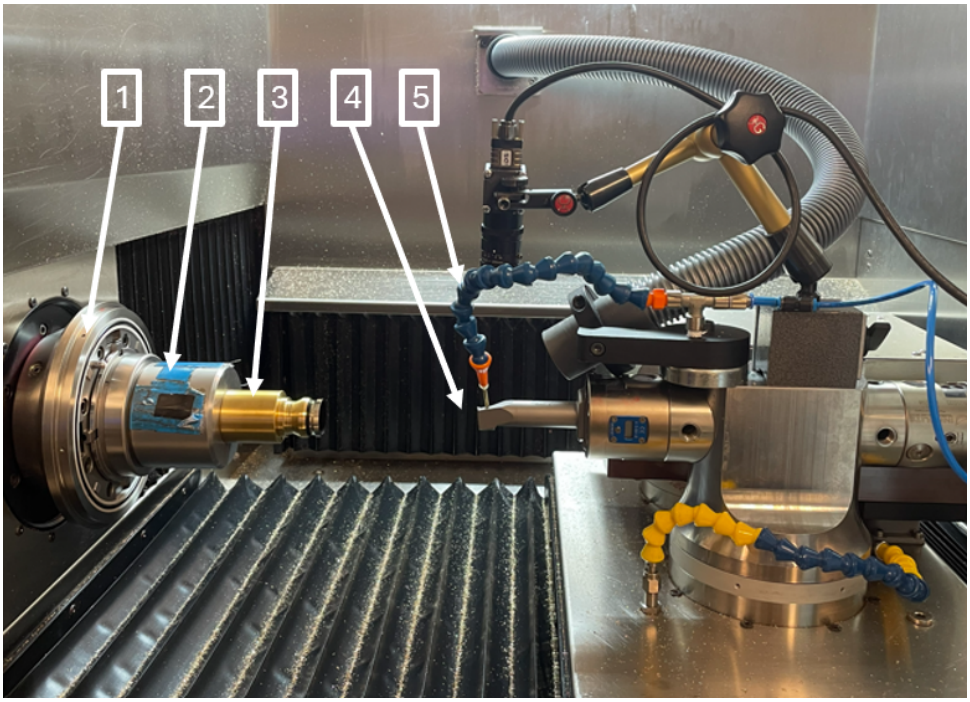

Figure 32: The main components of the turning machine. 1. Spindle. 2. Workpiece holder. 3. Workpiece. 4. Diamond cutting tool. 5. Cooling air supply.

Depending on the direction and surface to be machined, the tool will upon impact exert a torque on the barrel in the fixture. Since the current barrel is mounted using a thread, this torque can cause the barrel to be unscrewed. This could be corrected by changing the tool setup. However, Thorlabs prefers to have a solution independent of tool setup, since all changes regarding tooling negatively affect setup time and productivity. Additionally, a new tool holder would be too expensive. The consequence is that the barrel must be able to withstand the torque from the cutting tool without unthreading. In the case of a solution not based on a thread, the barrel must counteract the cutting force without sliding.

Due to complexities in determining cutting forces, an experimental approach was used to map the demands from machining. It was from company experience known that the barrel would be properly fixed during machining when the screw was tightened by 45-50 degrees. This amount of tightening is therefore more than enough to counter the torque from the cutting tool. If evaluated, this would provide a lower limit for the torque exerted on the barrel. This did not yield the lowest torque, but rather a design limit that had already been assured to work in practice. In order to find this torque, an experimental setup was built. The barrel was mounted in the fixture and clamped according to current operating procedure, meaning the screw was tightened by 45 degrees. The fixture was then mounted in a vise, and a rigid bar was connected

to the barrel. A metal cylinder of known mass, 1508 grams, was attached so that it could freely slide over the bar. This weight system was then carefully moved from the barrel edge outwards. When slipping occurred, the position on the rod was marked and measured. This procedure was repeated three times with five different barrels for increased statistical precision. The experimental setup is presented in figure 33.

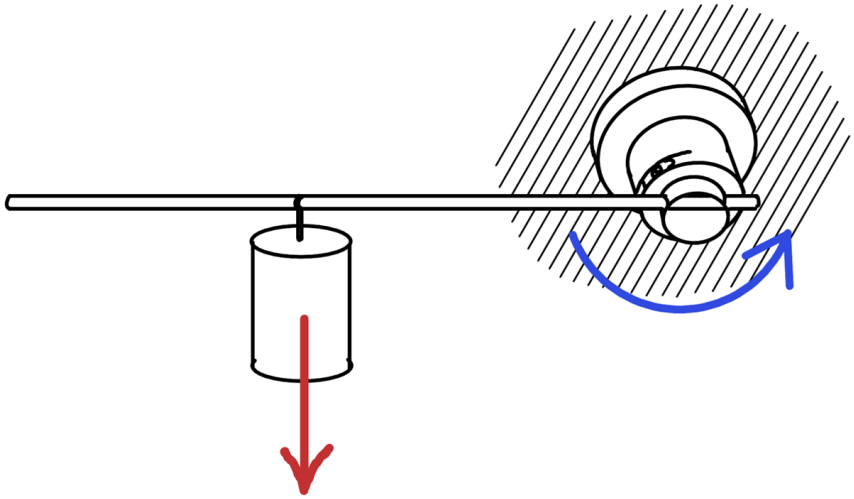

Figure 33: Setup for torque experiment

The torque experiments resulted in values for length, which were used for calculating the corresponding torque. The torque values for each test of each barrel are presented in table 2.

Table 2: Corresponding torque values in Nm for the measured lengths.

	Barrel 1	Barrel 2	Barrel 3	Barrel 4	Barrel 5
Test 1	2.6	1.3	3.3	2.9	1.1
Test 2	2.2	1.3	2.7	3.3	0.8
Test 3	1.9	1.3	2.9	3.9	1.1

The lowest torque value from the experiment was 0.8 Nm. It was possible that an even lower torque would be acceptable, but the challenge to determine this lower limit was too great. Instead 0.8 Nm was used as reference when applying loads for possible solutions.

3.3 Investigate other solutions

The torque experiment generated a lower limit for the torque that had to be counteracted. This torque was 0.8 Nm. This, along with a maximum allowable deformation in the barrel, constituted two clear design requirements. The allowed deformation was a cylindricity of 5 μm.

Additional objectives to be minimized were mounting time and cost. The investigated concepts were evaluated based on these constraints.

3.3.1 Three Jaw Chuck

The perhaps most common way to hold a workpiece in a turning machine is with a three jaw chuck. This type of chuck is in theory self centering, since all jaws are connected to a spiral scroll plate. By turning a drive gear with a wrench, the jaws will simultaneously move in radial direction and clamp the workpiece.

A common disadvantage of three jaw chucks is their inability to correct runout. Since the jaws are simultaneously connected to the scroll gear, they cannot be independently adjusted. If chips or dirt enter the mechanism, or in the case of uneven wear or play, the chuck axis will deviate from the theoretical true axis. These mechanisms will also affect self centering and repeatability, all of crucial value to the project investigated. Additionally, the challenge of fastening a new three jaw chuck to the machine must be addressed.

A way around this innate drawback is to use a system developed by the manufacturer of the turning machine at Thorlabs. This system has both an ultra high precision interface, allowing repeatable mounting on a nanometer scale. This would eliminate the need of developing a solution for connection to the machine. The chuck also has an additional alignment system for adjustment of the turning axis. Thanks to the alignment functionality, the necessary precision should be achievable, but must be verified. The issue with repeatability regarding workpiece mounting must also be verified.

An initial calculation to find necessary clamp forces was conducted. The three jaw chuck exerts three clamp forces on the workpiece, symmetrically spaced with 120 degrees between. By the Coulomb model, the friction force is related to the normal force, by equation 2. Here, F is the normal force from the jaws and $F_{friction}$ is the friction force that counteracts relative motion. The friction coefficient, μ, is set to 0.5 (The Engineering ToolBox, 2004). With a free-body diagram in the steady state of operation, the external force can be connected to the torque, calculated in section 3.2. The torque, $M = 0.8\,\mathrm{Nm}$, caused by the cutting tool is counteracted by three friction forces acting on a distance r from the center. The distance $r = 0.016245\,\mathrm{m}$ is half the maximum diameter of the barrel. This relation is presented in equation 3.

$$F_{friction} = \mu F \tag{2}$$

$$M - 3F_{friction}r = M - 3\mu Fr = 0 \rightarrow F = \frac{M}{3\mu r} \tag{3}$$

The calculated value for the external force was conservatively rounded up to $F = 34\,\text{N}$. With the forces, a simulation could be set up in Ansys. The current version of the TL15X was chosen for evaluation. The barrel was fixed axially with a frictionless support and the other degrees of freedom were constrained with a fixed support on a remote point located on the axis of rotation. The forces were added as line forces on the contact surface, 120 degrees apart each other. Deformations in a cylindrical coordinate system were evaluated at several heights, in order to get radial deformations. The Ansys setup is presented in figure 34. The simulation was also repeated with twice the force, $F = 68\,\text{N}$, to confirm that some variation in the applied force was acceptable.

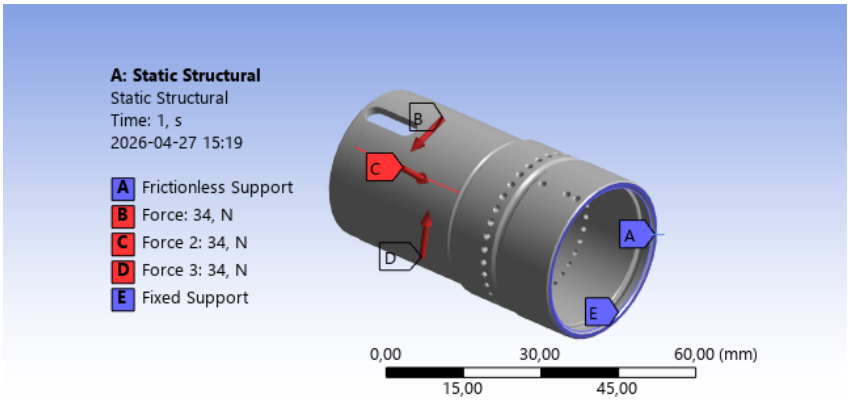

Figure 34: Setup of boundary conditions for the three jaw chuck in Ansys

The barrels did not deform significantly, but the resulting shape was profoundly triangular. The cylindricity was approximately $1.3\,\mu\text{m}$ for an external force of $34\,\text{N}$. Even with double the necessary force, the cylindricity was around $2.6\,\mu\text{m}$. Plots of the deformed barrels are presented in figure 35 and figure 36.

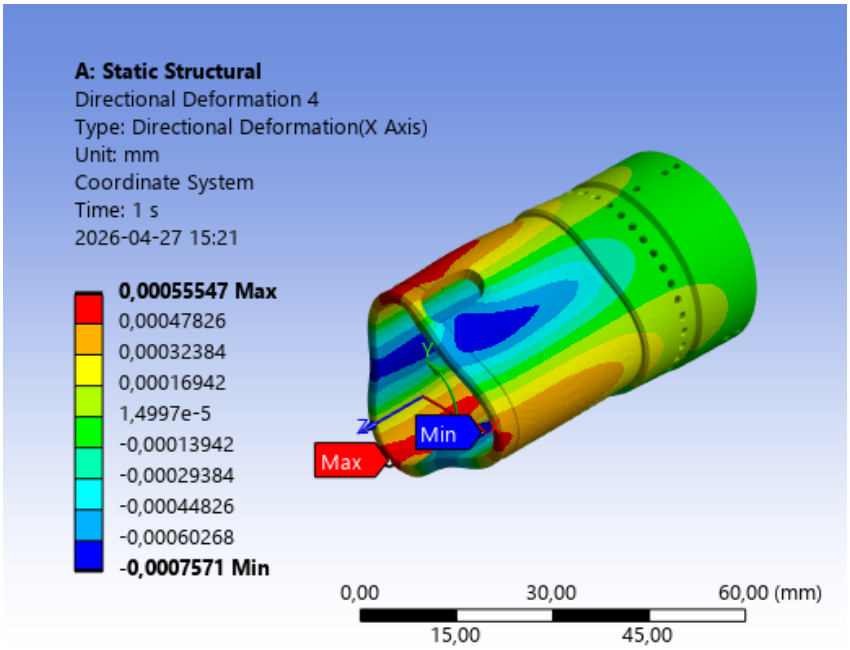

Figure 35: Three jaw deformation with an external force of 34 N

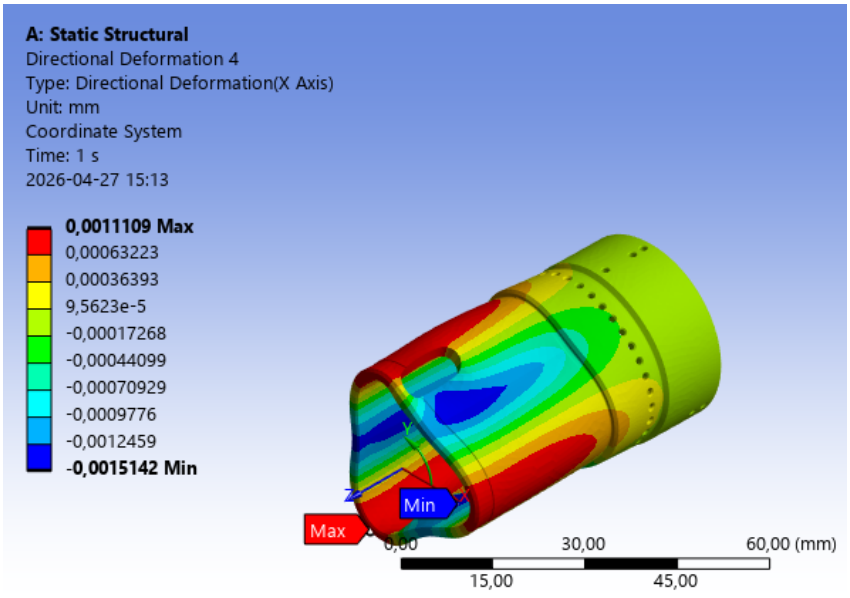

Figure 36: Three jaw deformation with an external force of 68 N

The calculations indicated viability of the solution. Since the machine specific three jaw chuck was already in possession, the setup procedure could be tested. The machining operator confirmed that proper tilt alignment on microscale was possible. However, the process required several iterations where the rotation axis was controlled by the turning machine interface when the workpiece is rotated but no material was removed. Improper alignment was then adjusted with the chuck screws and the process was repeated until the system is properly aligned. This

process took at least 15-20 minutes, which must be repeated for every unit due to the tolerances of the outer surfaces. As described in 1.2, mounting time is to be minimized. The necessary alignment time is therefore assessed as too long and the three jaw chuck is not a viable solution for serial production.

3.3.2 Clamp collet with relief

A simple solution for improving non-symmetrical clamping is to make relief cuts over the clamp. This has been tested in other precision engineering applications, for instance by Robert Campbell when fixing lenses in clamp mounts (Campbell, 2016). This method could potentially be implemented on the current fixture with a modifying machining operation. The potential of this solution was investigated with a FE-simulation. The CAD-model of the current fixture was modified with a larger free cut and additional relief cuts over the inner surface. Instead of a 10 mm cut perpendicular to the outer surface, a 305 degree circle sector-shaped cut was made around the cylinder. The cut would therefore be along the radius, which makes the cross section of the bent material more uniform over the fixture. The relief cuts were made with a similar shape to the clamp made by Campbell, as shown in figure 37.

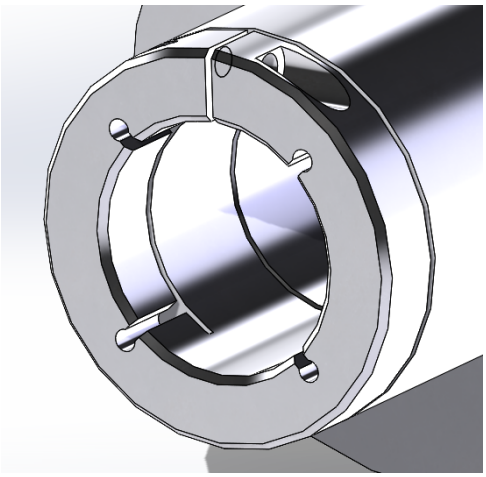

Figure 37: Relief cuts in the clamp area

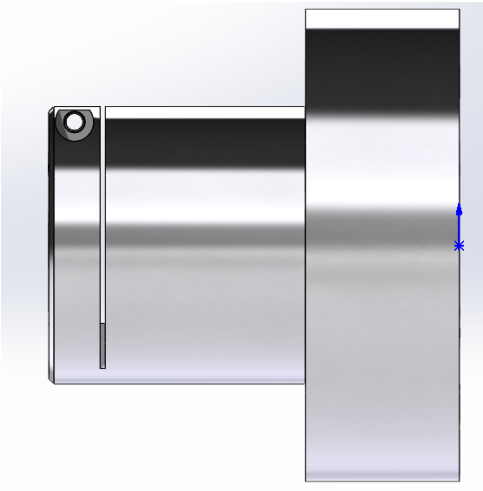

Figure 38: Increased cut for the clamp, viewed from the side

The exact dimensions of the reliefs were assessed to be of less importance. The goal with the simulation was instead to evaluate the mode of deformation and compare it to the current fixture. In the case of a promising result, work to optimize the cuts could be initiated. The revised 3D-model was imported to Ansys, and the same loads, contacts and boundary conditions as for the simulation of the current fixture were applied. Deformations in cylindrical coordinates at the same heights as before were evaluated and compared.

Compared to the simulation results of the original fixture, the clamp with relief cuts showed a more even deformation. Still, the deformation was not circular in nature. The barrel did instead get an oval shape and a prominent waist, where the clamp was applied, as shown in figures 39 to 41. The more even pressure distribution also improved runout values. Compared with height 2 from the original fixture, the runout was improved from approximately 0.016 mm to 0.011 mm.

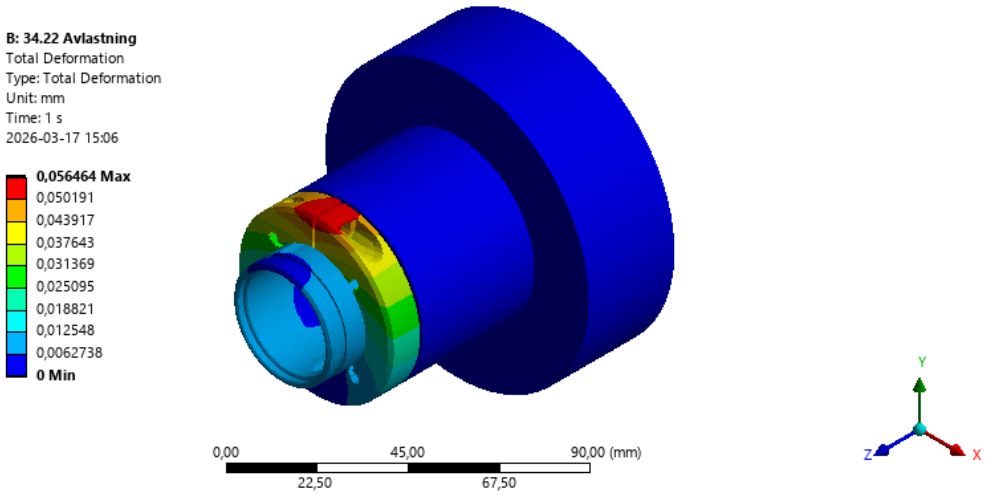

Figure 39: Unscaled deformation plot of the barrel in the fixture with relief cuts

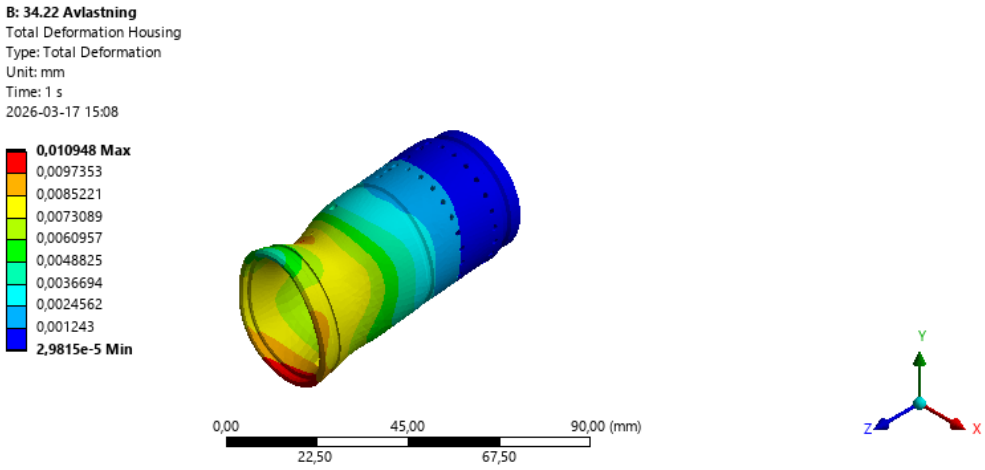

Figure 40: Scaled deformation plot of the barrel

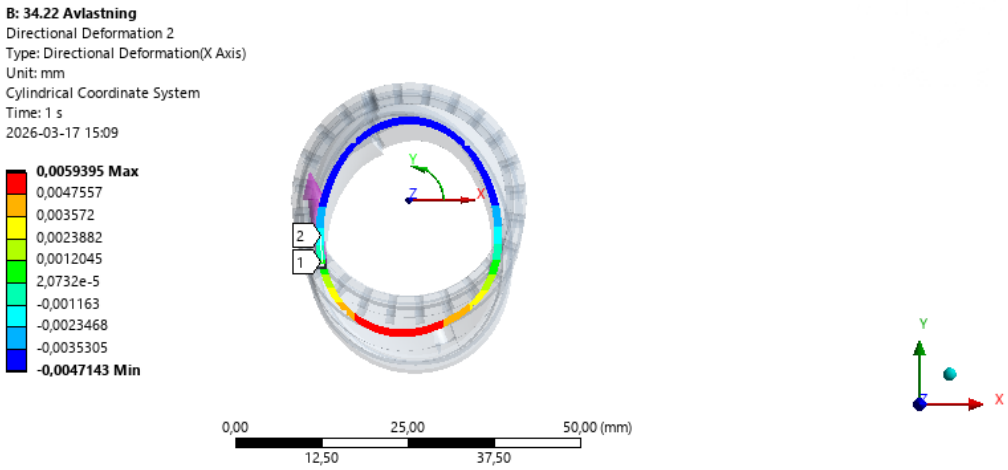

Figure 41: Scaled deformation plot of radial deformations at height 2 of the barrel

Due to the initial improvement, a second iteration was done with the relief cut principle. This time with a clamp that was doubled in length to mitigate the waist from the first iteration. This adjustment improved the waist-effect, but the runout value at height 2 was slightly worse. The effect of a longer clamp with relief cuts is shown in figures 42 to 44.

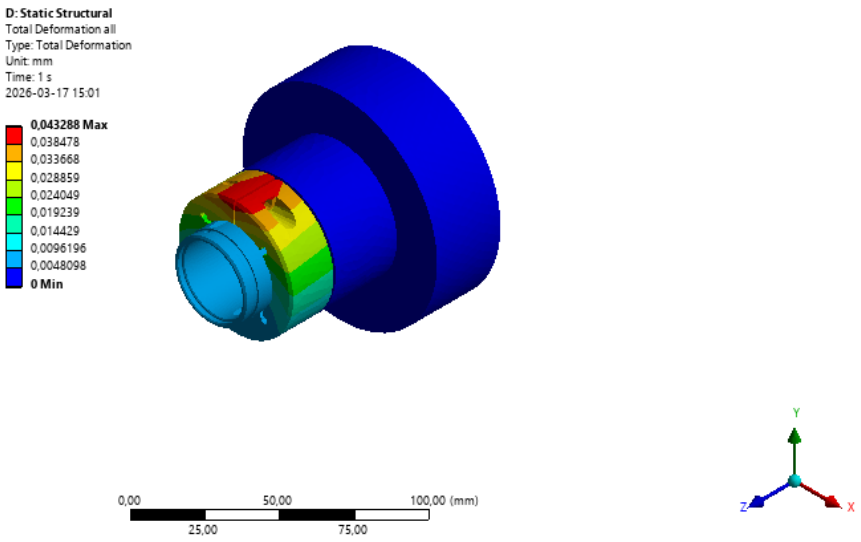

Figure 42: Unscaled deformation plot of the barrel in the fixture with a long clamp with relief cuts

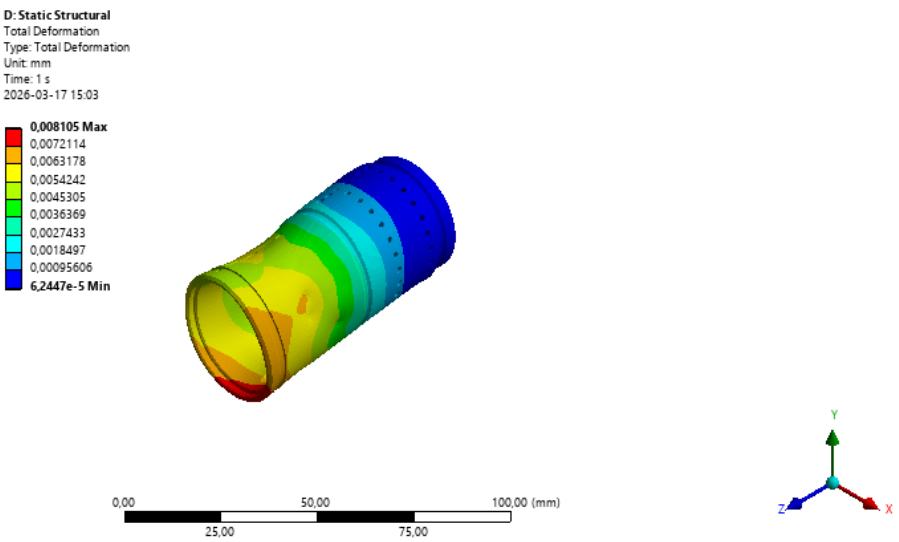

Figure 43: Scaled deformation plot of the barrel in the fixture with a long clamp with relief cuts.

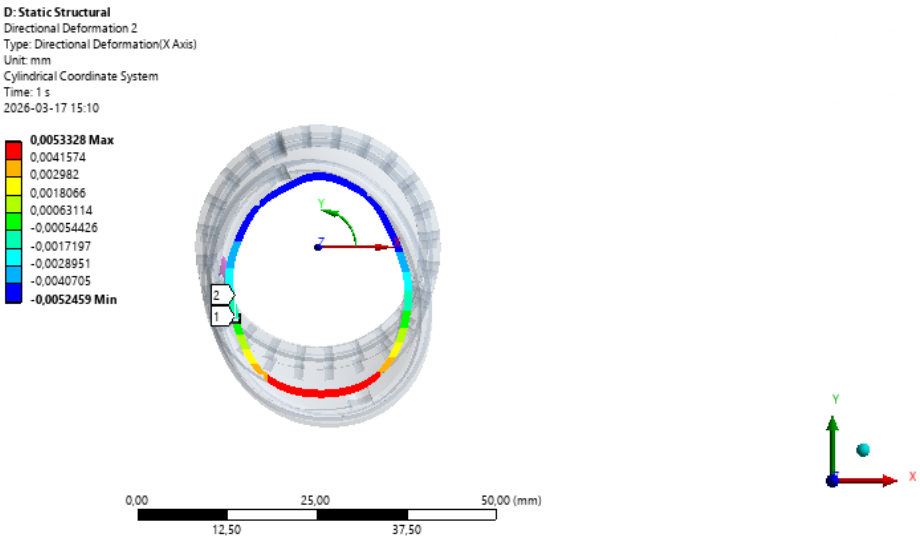

Figure 44: Scaled deformation plot of radial deformations at height 2 of the barrel in the fixture with a long clamp with relief cuts

In conclusion, a clamp with relief cuts reduces the deformation, both in form and in magnitude compared to the current fixture. The deformed shape is oval, but quite smooth around the barrel. With further optimization of the fixture, an acceptable magnitude of deformation might be achievable. It would still require substantial work since the initial simulation was more than twice as deformed as the accepted level of 5 μm in cylindricity. Even with a working simulation, the alteration must be implemented in reality as well. This is likely to take time and

require some changes with a machine shop involved. In summary, a fixture with an asymmetric clamp is fundamentally unsuitable for this application and the relief clamp can be dismissed.

3.3.3 Commercial ER-collets

An intuitive solution for limiting uneven stresses in workpiece holding is to increase the number of contact points around the circumference. This has for example been studied in bearing rings by Patalas et. al (Patalas et al., 2018). In commercial applications, this can be achieved by increasing the number of jaws in a conventional chuck, or by using so called ER-collets. These collets are conical with slits to alleviate uneven stresses. When compressed with an axial force from a nut, the conical shape will radially compress, thus fixing the workpiece or tool for the machining operation. ER collets are ISO-standardized and thus widely available and relatively cheap. An ER-collet is presented in figure 45. The functioning parts of an assembled collet chuck and the compressing forces on the collet are presented in figure 46.

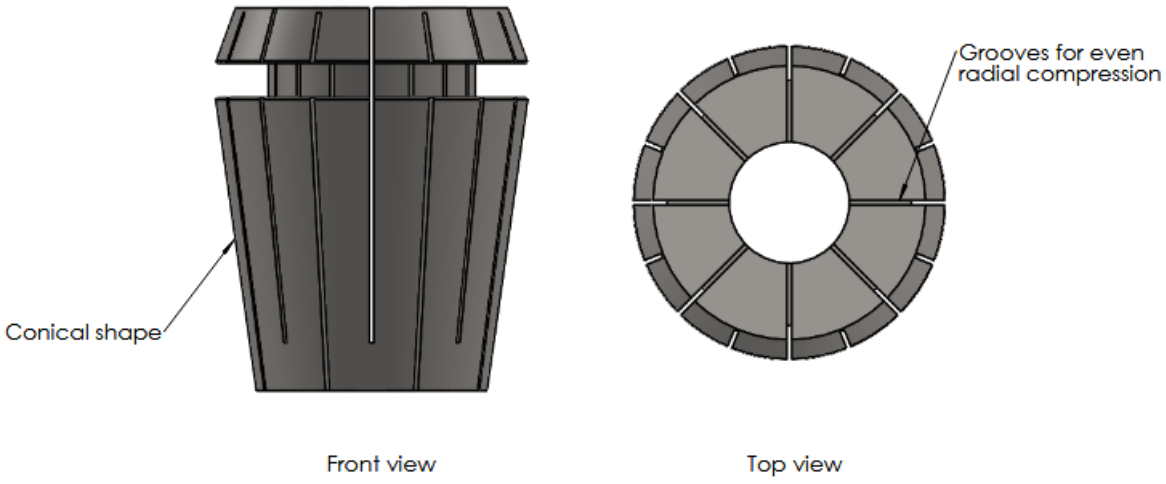

Figure 45: A standard ER-collet

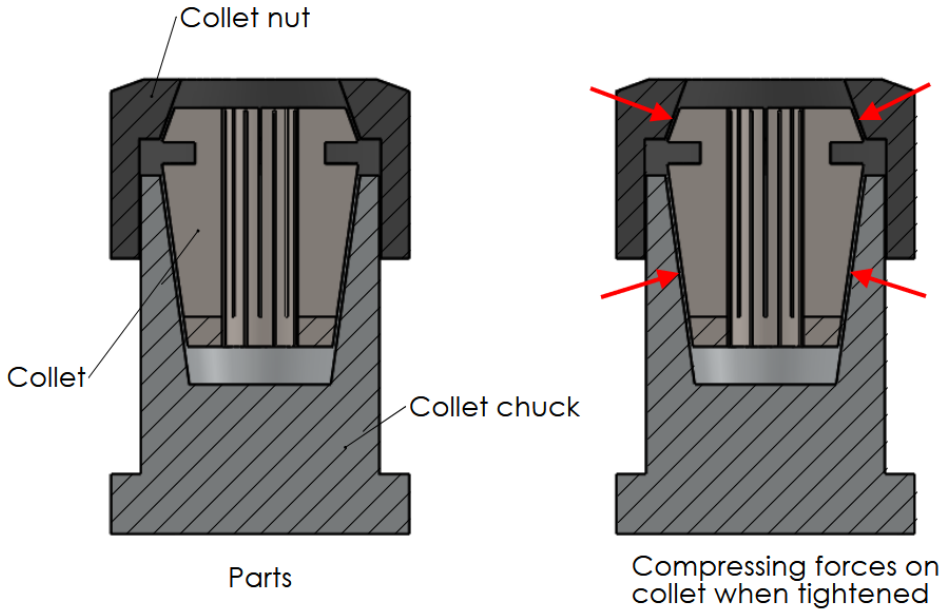

Figure 46: Concept sketch of an ER-collet chuck and the effects of tightening the nut

Evaluation of the ER-collet was done by physical testing. By doing so, the interpretation from a ”perfect”, virtual FE-setup to an imperfect reality was not necessary. The downside of this strategy was that the available ER-collet was slightly too small for the original iteration of the TL15X-barrel. Instead, the similar LMUL barrel with a diameter of approximately 32 mm was used.

The barrel was mounted in the collet and the collet holder was placed in the CMM machine. The barrel was first measured with no applied force from the collet nut. The nut was then tightened with a fixed angular value, until it was securely fastened. Measurements at the same heights were conducted at each level of tension, and values for cylindricity were evaluated.

The cylindricity was compared between the unclamped and clamped state. The resulting change, Δ Cylindricity was used as the evaluation value. This value needed to be below 5 μm, in order for the ER-collet to be a viable solution. In combination with the value, the deformed shape was evaluated. These values and corresponding shapes are presented in table 3. Figures 47 to 49 show the deformed shapes.

Table 3: ER-collet cylindricity

Measurement	Δ Cylindricity [mm]	Shape
1	0.004	Egg
2	0.0013	Circle
3	0.002	Triangle
4	0.004	Egg
5	0.004	Egg
6	0.003	Circle
7	0.003	Egg
8	0.004	Egg
9	0.005	Egg
10	0.006	Egg

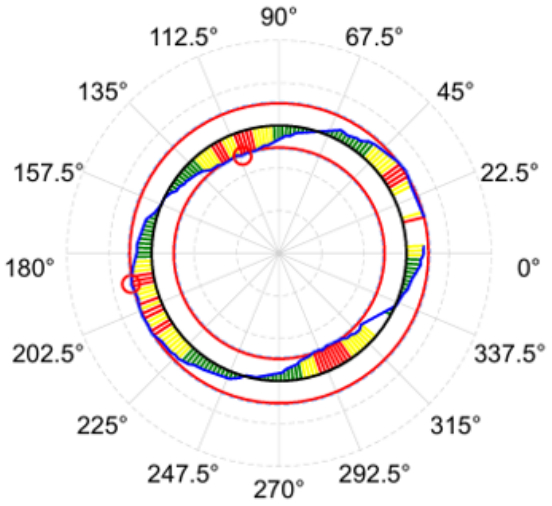

Figure 47: Deformed egg-shape

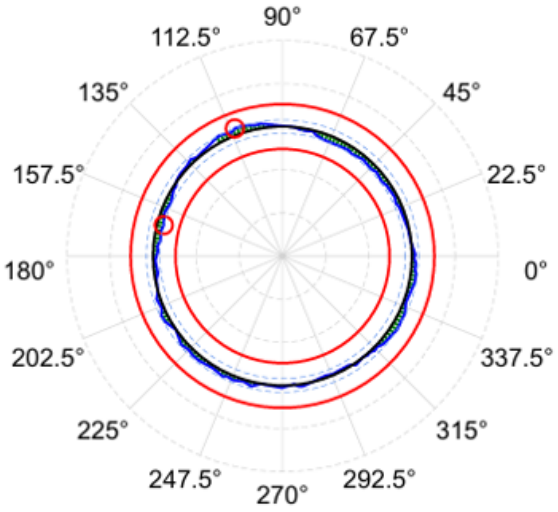

Figure 48: Deformed circle-shape

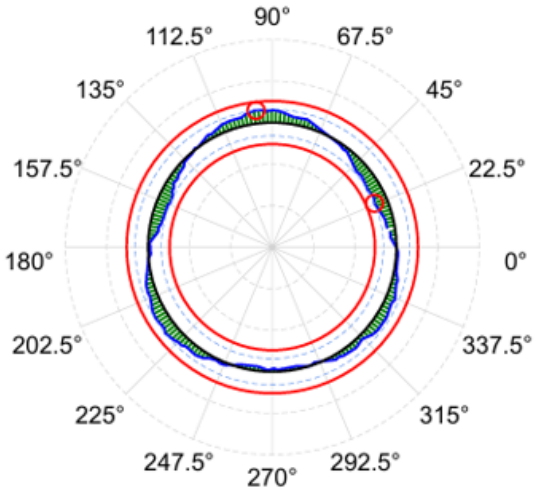

Figure 49: Deformed triangle-shape

As shown by the measured values, ER-collets could achieve a very small deformation. The smallest deformation measured was 0.0013 mm with an profoundly circular shape. The mean Δ Cylindricity was however just above 0.0036 mm, with a largest value of 0.006 mm. The deformed shapes were in most cases (8 out of 10) not round, which would be an issue in later production steps. The poor repeatability, in combination with the odd shapes and the possibility of relatively high deformation makes the ER-collet unsuitable for the application.

3.3.4 Shrink fit assembly

A theoretical method for attaining a perfectly symmetric clamping pressure is with a shrink- or press-fit. A shrink fit utilizes the thermal expansion of a material. When heated, materials expand, making assembly of an interference fit possible. When cooled, the parts become strained and form a secure joint. This joint allows for torque transfer with secure control of pressure. The pressure is not dependable of the uncertainties in, for example, a thread. Shrink fit assemblies rests on a solid theoretical ground, making calculations of necessary parameters relatively easy. The lower limiting factor for this application is to resist the torque measured in the experiment presented in section 3.2. The upper, limiting factor is either a maximal stress or the radial deflection of the barrel, caused by the external pressure. The theory and equations are gathered from *Maskinelement* (Mägi et al., 2017).

The barrel to evaluate was the newer model of TL15X. This version is similar to the one initially tested and simulated, but with incrementally increasing diameter. Firstly, the interacting surface was chosen as the largest outer diameter, due to its relative lack of weakening features such as slots and threaded holes. Both barrel and fixture was treated as ideal, hollow cylinders for the calculations. Calculation parameters for the barrel and hub are presented in tables 4 and 5. The barrel (hollow axle) material was the Brass-alloy, CW724R. The hub material was 6026 LF aluminium. The material data was gathered from manufacturer data sheets, see (Alumeco, n.d.-a) and (Alumeco, n.d.-b).

Table 4: Axle Parameters

Parameter	Explanation	Value
d	Nominal outer diameter	0.0325 m
d_{max}	Maximal outer diameter	0.032491 m
d_{min}	Minimum outer diameter	0.032475 m
d_0	Inner diameter	0.0285 m
L	Clamped length	0.0125 m
μ	Friction coefficient	0.1
ν_a	Axle poisson ratio	0.33
α_a	Axle thermal expansion coefficient	20 10^{-6}/K
E_a	Axle Young´s Modulus	110.3 GPa
σ_y	Axle yield limit	300 MPa

Table 5: Hub Parameters

Parameter	Explanation	Value
d	Nominal hub diameter	0.0325 m
D	Outer hub diameter	0.06 m
α_n	Hub thermal expansion coefficient	23.4 10^{-6}/K
E_n	Hub Young´s Modulus	69 GPa
ν_n	Hub Poisson ratio	0.31

The necessary force to counter the cutting torque was calculated using equation (4). The torque value used was 0.822 Nm, as measured in 3.2, and is expressed with M in equation 4. The force acts on a distance of half the diameter of the barrel. The calculations were made with both the maximum and minimum diameters provided by the tolerance of the part.

$$F = 2 * \frac{M}{d} \tag{4}$$

The corresponding surface pressure, p, for this calculated force was then calculated using equation 5. The friction coefficient in the equation, μ, was set to 0.1 for conservative reasons. Previous experiment has indicated that the friction between the fixture and barrel is high. However,

a shrink-fit fixture could be manufactured with a final pass in the ultra fine turning machine, leading to smooth surfaces. The smooth surfaces would most likely lower the friction, but with an unknown magnitude. πdL is the area affected by the pressure. The rearranged expression used for pressure calculation is presented in equation 6

$$F = \mu p \pi d L \tag{5}$$

$$p = \frac{F}{\mu \pi d L} \tag{6}$$

The equivalent von Mises stress, $\sigma_{e,max}^{v.M}$, used for the upper limit of the shrink fit is related to the yield strength, σ_y, with a safety factor of 2. This relation is presented in equation 7.

$$\sigma_{e,max}^{v.M} = \frac{\sigma_y}{2} \tag{7}$$

The equivalent stress is then calculated with equation 8, which is rearranged to equation 9. κ_a is the relation between the outer and inner diameter of the hollow cylinder axle, shown in equation 10

$$\sigma_{e,max}^{v.M} = \frac{2p}{(1-\kappa_a^2)} \tag{8}$$

$$p = \frac{\sigma_{e,max}^{v.M}(1-\kappa_a^2)}{2} \tag{9}$$

$$\kappa_a = \frac{d_0}{d} \tag{10}$$

Since the upper limit is controlled either by the stress of the barrel or its radial displacement, a displacement relation is necessary as well. This relation is presented in equation 11 and is rearranged to equation 12. Here, u represents the radial displacement, ν_a is the poisson ratio of the barrel and r is the radial coordinate. The radial coordinate is the distance from the center axis to the machined surface. The maximum radial deflection for this surface is limited to 2.5μm. A notable detail is that the diameter change is expressed as $2u$. Also, the minus sign

in the equation indicates a compressive pressure. The magnitude from this equation is what is used in the grip calculation, in equation 14.

$$u = -\frac{pr}{E_a} * \frac{(1-\nu_a) + \kappa_a^2(1+\nu_a)(d/2r)^2}{1-\kappa_a^2} \tag{11}$$

$$p = -\frac{uE_a}{r} * \frac{1-\kappa_a^2}{(1-\nu_a) + \kappa_a^2(1+\nu_a)(d/2r)^2} \tag{12}$$

With the limiting parameters calculated, the interference can be determined. All parameters can be found in tables 4 and 5, combined with earlier equations. The remaining parameter κ_n, the relationship between the outer and inner diameter of the hub, was determined with equation 13

$$\kappa_n = \frac{d}{D} \tag{13}$$

$$\Delta = pd\left[\frac{1}{E_n}\left(\frac{1+\kappa_n^2}{1-\kappa_n^2} + \nu_n\right) + \frac{1}{E_a}\left(\frac{1+\kappa_a^2}{1-\kappa_a^2} - \nu_a\right)\right] \tag{14}$$

Since the outer diameter of the barrel was constrained by a g6 fit, the calculation had to be made with the different extreme values in mind. The g6 fit indicates that the actual diameter deviates from the nominal diameter within a fixed tolerance determined by an ISO-standard. In this case the upper limit was the nominal diameter minus $9\,\mu$m and the lower limit was the nominal diameter minus $25\,\mu$m The diameters used were therefore $d_{min} = 0.032475\,$m and $d_{max} = 0.032491\,$m

The force calculation in equation 4 gave the necessary force to counter the machining force. For the smaller diameter, the force was $F_{d,min} = 50.62\,$N. For the larger diameter, the force was $F_{d,max} = 50.6\,$N.

With the calculated forces, the minimal pressure necessary to avoid relative motion was determined with equation 6. The result was a minimal pressure of $p_{d,min} = 396.77\,$kPa and $p_{d,max} = 396.58\,$kPa.

The safety factor for yield was set to 2, meaning the maximum effective stress for the assembly

is half the yield stress. With equation 7 this was calculated to $\sigma_{e,max}^{v.M} = 150\,\text{MPa}$.

The diameter relations from equation 10 and 13 was also calculated. This resulted in the following diameter ratios:

- $\kappa_{a,d,min} = 0.8776$
- $\kappa_{a,d,max} = 0.8772$
- $\kappa_{n,d,min} = 0.5413$
- $\kappa_{n,d,max} = 0.5415$

With all the necessary input data determined, the pressure limited by both allowed stress and deflection could be calculated. The continued use of maximum and minimum outer diameter resulted in the following values from the stress and deviation limitations in equation 9 and 12:

- $p_{stress,d,min} = 17.25\,\text{MPa}$
- $p_{stress,d,max} = 17.325\,\text{MPa}$
- $p_{disp,d,min} = 2.32\,\text{MPa}$
- $p_{disp,d,max} = 2.33\,\text{MPa}$

The calculated values show that the limiting factor is displacement. The barrel will deform more than the allowed amount before a critical stress is achieved. The maximum pressure is therefore governed by p_{disp}.

Finally, the necessary grip could be determined from the maximum and minimum pressures, using equation 14. The resulting values were as follows:

- $\Delta_{min} \approx 1.3\,\mu\text{m}$
- $\Delta_{max} \approx 7.4\,\mu\text{m}$

In conclusion, the interference fit between the hub and barrel must be very small to avoid excessive deformation. The maximum allowed grip can only be $\Delta_{max} \approx 7.4\,\mu\text{m}$. Considering that the outer diameter has a tolerance magnitude of $16\,\mu\text{m}$, a shrink fit would not be possible with the current barrel dimensions. Furthermore, the maximum deviation would likely be larger than calculated, considering the weakening features around the barrel surface. The shrink-fit concept can be made possible with smaller tolerances on the barrel, in combination with

extensive quality control. In reality, this will increase costs and labor, and the shrink-fit concept can therefore be dismissed.

3.3.5 Axial compressive clamping

To completely bypass the problem of uneven stresses along the circumference of the barrel, the workpiece could be fixed with axial force. If the barrel is axially compressed between two surfaces, the friction force between the barrels end surfaces and the fixture could prevent unwanted sliding in the turning machine.

A fixture that connects to the turning machine and a nut that clamps the lens barrel to the fixture were developed in Solidworks. The nut threads onto the outside of the fixture and compresses the barrel. It also features a hole that allows for tool insertion. The concept can be seen in figure 50.

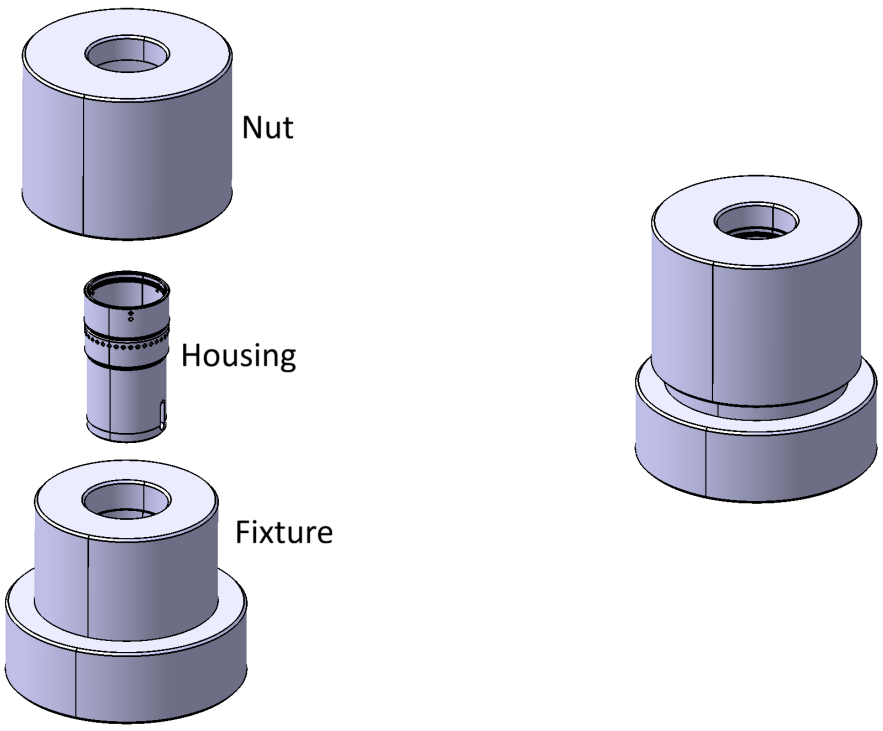

Figure 50: Initial concept for the axial clamp including the lens barrel

The required clamping force to prevent the barrel from sliding during operation was calculated using the results from the torque experiment described in section 3.2. From force and torque equilibrium applied to the barrel under processing in the turning machine, equations 15 and 16 were obtained.

$$\sum M = 0 \implies M_{exp} = M_1 + M_2 \tag{15}$$

$$\sum F = 0 \implies N_1 = N_2 = N \tag{16}$$

Where

- M_{exp} is the smallest torque where sliding occurred in the original fixture in the torque experiment
- M_1 and M_2 are the reaction torques caused by the frictional forces along the top and bottom edge of the barrel
- N_1 and N_2 are the axial reaction forces that the fixture and nut exerts on the barrel

Combining equations 15 and 16, and expressing the torque as a function of friction force times radius, yielded equation 17.

$$M_{exp} = \mu N r_1 + \mu N r_2 = \mu N (r_1 + r_2) \tag{17}$$

where r_1 and r_2 are the medium radii of the top and bottom of the lens barrel.

Rearranging to solve for the axial force gave equation 18.

$$N = \frac{M_{exp}}{\mu (r_1 + r_2)} \tag{18}$$

where

- $M_{exp} = 0.822$Nm
- the frictional coefficient $\mu = 0.08$
- $r_1 = 0.02815$m
- $r_2 = 0.03125$m

This resulted in a required axial force of 172.98 N. This force would be regulated by controlling the torque to tighten the nut onto the fixture. The nut tightening torque was calculated using

equation 19 (Mägi et al., 2017). The use of M_{exp} as a limit for the induced torque from the turning process in combination with a conservatively chosen friction coefficient results in some unknown safety factor.

$$M_{inst} = N(0.16P + 0.58\mu d_2 + \mu r_2) \tag{19}$$

The torque required to remove the nut was calculated according to equation 20.

$$M_{rem} = N(-0.16P + 0.58\mu d_2 + \mu r_2) \tag{20}$$

where

- P is the thread pitch
- d_2 is the pitch diameter

M_{rem} (0.94 Nm) turned out to be greater than M_{exp}. This means that the friction in the thread would be enough for the nut to not unscrew itself during processing of the barrel.

To improve the confidence in the viability of the concept, a static structural simulation was run in Ansys. In the simulation, the force, N, was multiplied by 4 to ensure a large margin against unacceptable deformation in the barrel as a result from clamping.

The simulation was similar to those conducted on the original fixture. All contacts was set to frictional with a coefficient of friction of 0.08. This number was chosen to not exceed measured values of the coefficient of friction of brass on brass (Chowdhury et al., 2012). The holes in the bottom of the fixture that are meant to interface with the turning machine were pinned with fixed supports, and a force was applied in the thread of the nut, clamping the barrel. The boundary conditions are illustrated in figure 51.

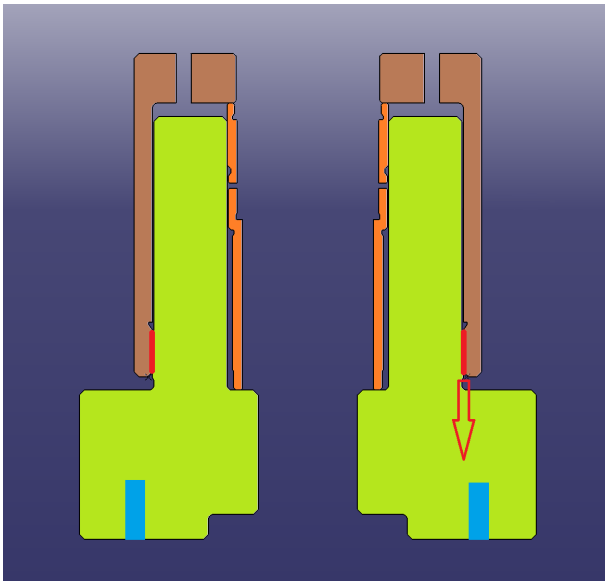

Figure 51: Cross-sectional view of the nut (brown), barrel (orange) and fixture (green). The force is represented in red and the fixed support in blue

The resulting deformations from the simulation is shown in figure 52.

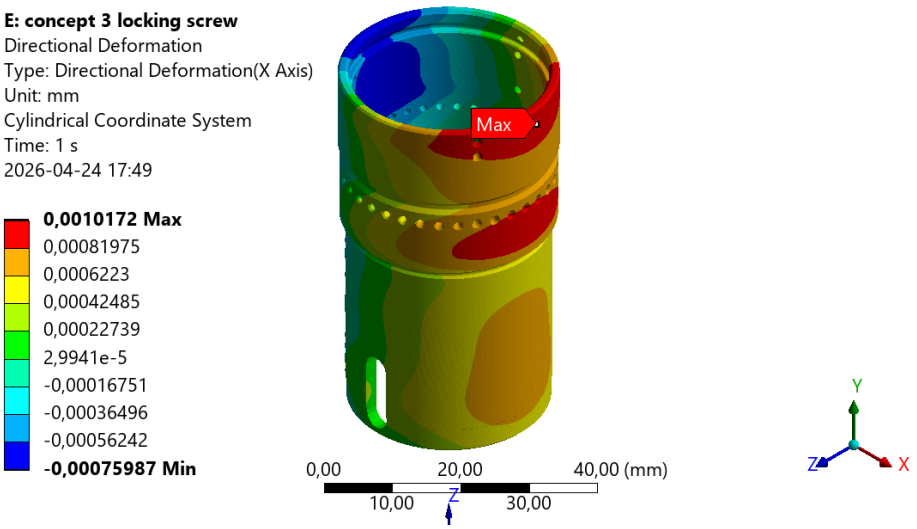

Figure 52: Radial deformation of the lens barrel

The simulated deformations resulted in a cylindricity of $\sim 1.8\,\mu$m. This does not exceed the tolerance of $5\,\mu$m which proves the concepts viability.

To ensure that the axial clamp would not be over or under tightened, the nut needed to allow the use of a torque wrench. Since there was no easy way to interface the type of torque wrenches that control sufficiently small magnitudes of torque, an adapter to fit over the hole in the nut was designed. The adapter is attached to the top of the nut using steel guide rods and features a

central threaded hole that fits an M4 screw. The head of the screw acts as the connection point for the torque wrench and can be easily swapped if worn out. The adapter setup can be seen in figure 53.

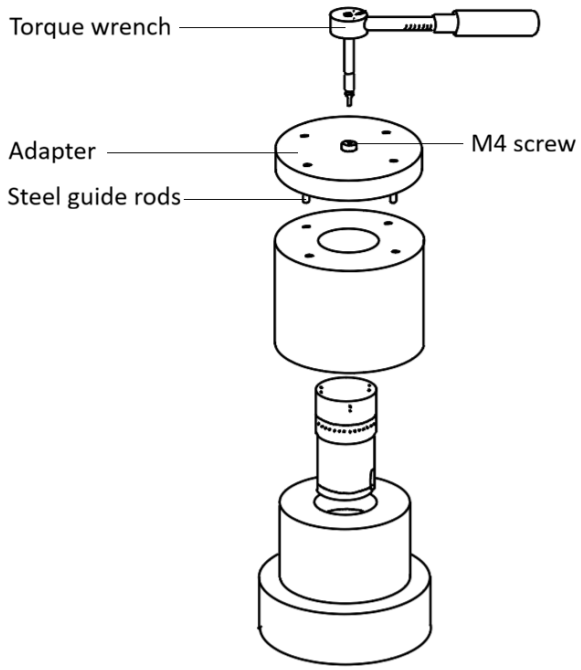

Figure 53: The nut, adapter and torque wrench

4 Results

Investigation utilizing FE simulation shows that the method of holding the lens barrel during turning is the root cause of the inadequate precision currently achieved. The asymmetrical clamp deforms the barrel elastically, resulting in rotational asymmetry. When the barrel is machined, adequate cylindricity is achieved, but when it is released from the fixture it ”springs” back as the stresses are released and stabilizes in a deformed state. This means that a principle of workpiece holding that introduces reduced, or more even radial stresses in the barrel can be a solution.

FEM-simulations and calculations show that among the five possible conceptual solutions investigated in this work, an axial clamp is the most viable method for workpiece holding in ultra-precision turning. Table 6 shows an evaluation of the concept solutions.

Table 6: Concept evaluation

Concept	**Deformation**	**Suitability**	**Comment**
Three jaw chuck	pass	fail	Setup time to long
Clamp collet with relief	fail	fail	
Commercial ER-collet	fail	fail	
Shrink fit assembly	pass	fail	Barrel tolerance is overly permissive
Axial compressive clamp	pass	pass	

4.1 The axial clamp

The most suitable concept for minimizing unwanted deformation during the turning process was the axial clamp. The clamp consists of a fixture that attaches to the vacuum chuck in the lathe and a nut that is threaded onto the fixture. The lens barrel is contained in a cavity in the fixture and clamped into place by the nut as seen in figure 54.

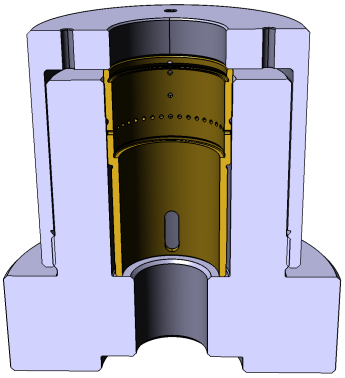

Figure 54: Sectional view of the axial clamp containing the lens barrel

The nut has a central hole on its top surface with a diameter matching that of the lens barrel. The hole allows for a cutting tool to be inserted. The top surface also has holes for guide rods that allow the nut to interface with an adapter disc. The adapter facilitates the possibility to use a torque wrench for tightening the nut. This ensures that the nut is not under-tightened and run the risk of unthreading during operation, and that the barrel is not overly compressed. The entire assembly is made of brass to allow for in house adjustments using machines that are not able to machine harder materials. Figure 55 and 56 shows the unassembled and assembled axial clamp.

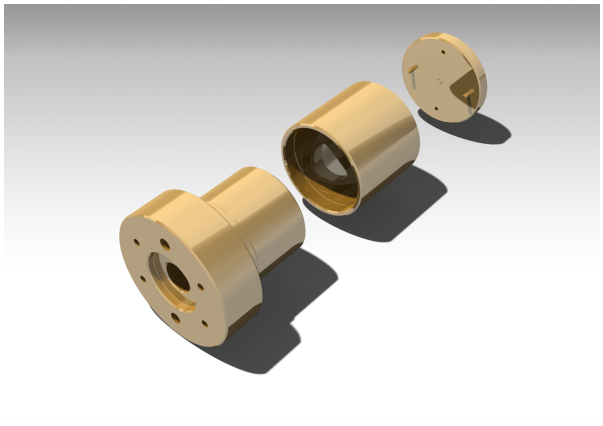

Figure 55: Fixture, nut and adapter

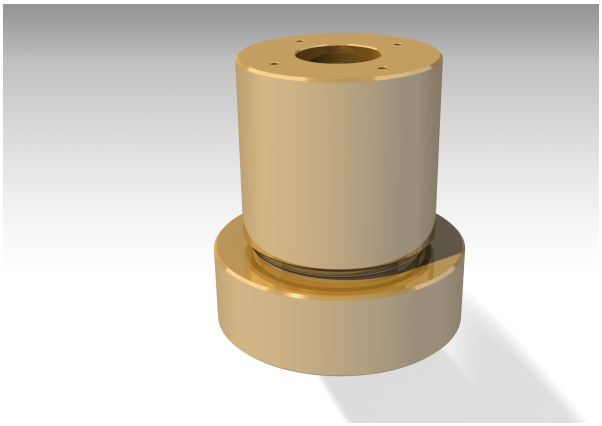

Figure 56: Assembled fixture and nut

4.2 Method validation

The result also proved that FEM was a viable method to find the cause of unwanted deformations in machining of lens barrels. FEM, in combination with conventional mechanical calculations, can also successfully be used in the construction and evaluation of new solutions

that reduce unwanted deformations while still resisting cutting forces from machining.

5 Discussion

This chapter addresses the challenges encountered, as well as reflections on the results, methods of the projects and suggestions for future research.

5.1 FE-model

The first phase of the project was the simulation of the current fixture. This was initially believed to have a profound impact on a new solution. However, the increased number of alterations and assumptions added to the model made it difficult to transfer the findings to the physical world.

Notably, the simulation matched the measured values best when using a rough friction formulation between the barrel and fixture, which was a surprising result. The reasoning before the simulation was that, since real world values for the frictional coefficient between brass and aluminium were not found, despite a thorough literature investigation, a value obtained from the simulation could replace it. Instead, the best result was achieved with a rough formulation, which could be explained by several causes. After examining the rough and scratched inside of the fixture, one theory is that load was transferred by form rather than frictional force. Still, the knowledge gained from working with friction indicates that it is a complex phenomenon, and precautions must be taken to avoid depending on an unknown variable.

Moreover, it was also noted that the radial displacement and thus the radial loads were the critical aspects of designing functioning workpiece holding solutions. Even the smallest applied torque on the screw in the original fixture from the measurement step in section 3.1 resulted in an unacceptable form of the barrel. This led to the intuitive knowledge that an improved fixture had to have an even and preferably low radial load, while still counteracting the cutting forces.

5.2 Experimental uncertainty and repeatability

Additionally, some notable objections to the FE-model must be lifted. Only one lens barrel was used in the optimization of the model comparing the simulation and the measured values. It is therefore not statistically valid to draw large conclusions about the validity of the model. The unmachined barrels have a dimensional variation that would most likely result in a variation in how they deform as well. The model did, however, match the deformation mode experienced

in production and provided general guidelines and ideas for improvement. The model also identified the fixture as the issue affecting the turning precision of the lens barrel.

Moreover, the torque test of section 3.2 contained some innate uncertainties as well. The tightening was done by a predefined angle, but the accuracy of this manual procedure can be questioned. The test showed a variation of over 370% between the smallest and largest holding torque. The smallest value was chosen as a machining demand, but the value variety indicates a large difference in load exerted on the barrel between different samples.

Lastly, the comparison between measurement and simulation was based on measurement from one height only. A potential drawback from this method is that the mapping of the complete barrel deformation is lost. The selected height was used due to its closeness to the largest deformation and the fact that it yielded datapoints around the whole circumference. A better comparison could have been generated by comparing datasets from all heights, but that was not conducted. However, the deformation field is continuous. This means that by optimizing the comparison based on the largest deformation, the deformation at other areas should be indirectly mapped as well. Still, a complete comparison would have been preferred.

5.3 Variation of barrels in evaluation

Several different lens barrels were used in the evaluation of different concepts. A previous version of TL15X was used for the main comparison between simulation and physical deformation and the relief clamp evaluation. A lens barrel for the LMUL objective was used in the ER-collet evaluation. For the shrink fit calculation, axial clamp and three jaw chuck, the current version of TL15X barrel was used. Since the aim was to improve the turning precision of the current TL15X barrel, usage of different barrels is a possible cause of error. However, the barrels were geometrically very similar. Additionally, the same type of machining error has previously been found in the inspection and production of all barrels. In combination, this led to the assessment that the result from evaluation of one barrel type could be transferred to the other types.

5.4 Comparison of fixture concepts

A relatively broad range of fixture concepts followed the FEM-modeling of the problem. The challenges from each concept also had a large variation, which were interesting to analyze.

The three jaw chuck showed a promising lack of deformation, despite introducing radial stresses. This was surprising, since the FEM-model of the current clamp indicated that even small loads in the radial direction could result in deformations above the limit. If not for the time needed to align the small scale deviations in the rotational axis, the conventional three jaw chuck would have been a sufficient solution for this high precision application.

A clamp collet with relief cuts showed an initial large improvement. It was however quickly evident that the fundamental flaws from the initial fixture, an asymmetrically applied load, was challenging to overcome. Compared to the initial fixture, the load was more evenly distributed. It was however difficult to achieve a perfectly distributed stress. An increased number of clamps could possibly improve the load distribution, but challenges in applying the load evenly would still exist. A screw based solution, with the inherent range of frictional values would cause uncertainties. A valuable insight from the work with the relief clamp was therefore to construct a solution with symmetry in applied loads with less dependency of friction.

Another conventional method was the commercially available ER-collets. In several measurements, the deformations remained under the limit, but the barrel showed a surprising level of form variation. Ideally, their geometry should result in an even radial compression, but the measured deformations were, in over half of the cases, unacceptably oval in shape. The differences in form deformations and thus the repeatability were a surprising result. This could be explained by the unpredictability in contact formulation and friction, previously noted in the iterations of the FEM-model. Another possible explanation for the insufficient repeatability is the manufacturing tolerances of ER-collets and the weakening features in the barrel. The tested LMUL-barrel have, for example, three axially oriented lines of closely spaced holes, that might explain the triangular shape.

The shrink fit concept stemmed from the realization that symmetric loads would result in more predictable deformations. The loads in the shrink fit would also depend on material parameters and temperature, two highly measurable and consistent parameters. This would reduce the dependency on thread friction in the load application. As shown by the initial FEM model and measurements, frictional contacts are difficult to predict and rely on. Calculations for the shrink fit concept could be performed without wide assumptions, based on the demands set by optical performance. The resulting small, necessary grip did however render the concept unsuitable for this application. The allowed variations in outer diameter in the barrel were

larger than the allowed grip, meaning that a shrink fit fixture could not be directly implemented for the current product. Logistically, the time for heating and cooling would also in reality be quite unpractical. For future fixtures with different outer tolerances, this concept could still be considered.

The concept chosen for improving the turning precision of the lens barrel was the axial clamp. It achieved adequate clamping force without introducing the problematic stresses. This concept was however still dependent on friction to counteract the machining forces. Interestingly, the simulation showed relatively small variations in deformation between different magnitudes of applied forces. This lack of variation meant that excessively large forces could be applied without exceeding the deformation limit. As a result, frictional forces in the thread and on the contact surfaces could be conservatively calculated with a small friction coefficient and still yield an adequate result. This lack of sensitivity aids in the mounting of the barrel by allowing a time efficient mounting process.

5.5 Future research suggestions

One important aspect for fixture design is, as discussed, evaluation of the limiting machining torque. By implementing theories for cutting force evaluation, different concepts for retaining the workpiece may be possible.

Another important aspect for production efficiency is to investigate the time spent for the machining process. For optimal production flow, mounting time is of the essence, and a fixture can be optimized based on this criterion.

Furthermore, it could be interesting to investigate the feasibility of the method of axial clamping in other similar products. Thorlabs produces multiple different lens barrels that could benefit from utilizing the same type of fixture. The production could also benefit greatly from a method that allows for the barrels to be machined both internally and externally in the same clamping.

References

AB Sandvik Coromant. (2021). *Metal Cutting Technology Training Handbook*. https://epublications.sandvik.coromant.com/frontend/getcatalog.do?catalogId=1154021&catalogVersion=1&lang=en

Alumeco. (n.d.-a). *CW724R* [fact sheet]. https://www.alumeco.com/media/b1xphhgz/cw724r_version1.pdf

Alumeco. (n.d.-b). *EN AW 6026 LF – rods and bars* [fact sheet]. https://www.alumeco.se/aluminium/stanger/rundstaang/en-aw-6026-lf/8-x-3000-mm/p/10001417/10137042

Campbell, R. J. (2016). *Split clamp design and analysis*. Practical Precision. https://practicalprecision.com/split-clamp-design-and-analysis/

Chowdhury, M. A., Nuruzzaman, D. M., Mia, A. H., & Rahaman, M. L. (2012). Friction Coefficient of Different Material Pairs Under Different Normal Loads and Sliding Velocities. *Tribology in Industry*, *34*(1), 18–23. www.tribology.fink.rs

Engineer Essentials LLC. (2026). *GD&T Symbols Reference Guide*. GD&T Basics. https://www.gdandtbasics.com/gdt-symbols/

Gallagher, N. B. (2020). *Savitzky-Golay Smoothing and Differentiation Filter*. Eigenvector Research Incorporated. https://doi.org/10.13140/RG.2.2.20339.50725

Kurowski, P. M. (2004). *Finite Element Analysis for Design Engineers*. SAE International. https://www.sae.org/books/finite-element-analysis-design-engineers-third-edition-r-541

Liebrich, T. (2024). *Ultra-Precision Turning*. RhySearch. https://www.rhysearch.ch/aktuelles/publikationen/whitepaper/ultra-precision-turning.html

Lin, T. Y., & Cheng, C. C. (2011). A novel opto-mechanical tolerance analysis method for precision lens systems. *Precision Engineering*, *35*(3). https://doi.org/10.1016/j.precisioneng.2011.02.001

Mägi, M., Melkersson, K., & Evertsson, M. (2017). *Maskinelement*. Studentlitteratur. https://www.studentlitteratur.se/kurslitteratur/teknik/maskinkonstruktion/maskinelement/

Möhring, H. C., Biermann, D., Bleicher, F., Melkote, S., & Kappmeyer, G. (2025). Fixtures and workpiece clamping systems in machining. *CIRP Annals - Manufacturing Technology*, *74*(2). https://doi.org/10.1016/j.cirp.2025.04.096

Patalas, A., Regus, M., & Peta, K. (2018). Studies of thin-walled parts deformation by gripping force during turning process on an example of bearing ring. *MATEC Web of Conferences*, *244*. https://doi.org/10.1051/matecconf/201824402010

Sunar, Ö. (2021). *Ansys contact types and explanations*. Mechead. https://www.mechead.com/contact-types-and-behaviours-in-ANSYS/

The Engineering ToolBox. (2004). *Friction - coefficients for common materials and surfaces*. https://www.engineeringtoolbox.com/friction-coefficients-d_778.html

Wang, Y., Yuan, Z., Wu, T., & Yan, H. (2021). Prediction of cutting force in ultra-precision machining of nonferrous metals based on strain energy. *Nanotechnology and Precision Engineering*, *4*(4). https://doi.org/10.1063/10.0005648

Yoder, P. R. (2008). *Mounting optics in optical instruments* (2nd). SPIE. https://doi.org/10.1117/3.785236

A Python code for comparison of CMM and Ansys values

```
1
2  import numpy as np
3  import matplotlib.pyplot as plt
4  from scipy.signal import savgol_filter
5
6  theta_ansys = np.loadtxt("Theta_ansys.txt") #import the angles
       from the simulation
7  theta_cmm = np.loadtxt("Theta_cmm_red.txt") #import the angles
       from the CMM (measured)
8
9  r_ansys = np.loadtxt("r_ansys.txt") #import the simulation radii
10 r_cmm = np.loadtxt("r_cmm_red.txt") #import the CMM radii (
       measured)
11
12 r_cmm_savgol = savgol_filter(r_cmm, 300, 2) #reduce the noice in
       the CMM radii
13
14 min_idx_ansys = r_ansys.argmin() #find the index of the smallest
       simulated radius
15 min_idx_savgol = r_cmm_savgol.argmin() #find the index of the
       smallest measured radius
16
17 #find the phase shift of the simulated and measured plots by
       finding the difference in angle for the smallest radii
18 anglediff = theta_ansys[min_idx_ansys] - theta_cmm[min_idx_savgol
       ]
19
20 #add the angle difference to the CMM values to align it to the
       simulated values
21 #if the sum exceeds a full circle (2 x pi) it is reduced by 2 x
       pi
22 n = 0
23 for i in theta_cmm:
```

```
    if i + anglediff > 2*np.pi:
        theta_cmm[n] = anglediff + i - 2*np.pi
    else: theta_cmm[n] = anglediff + i
    n = n + 1

max_idx_theta_cmm = theta_cmm.argmin() #find the cutoff in angle values where the circle completes a loop

#rearrange the measured radii and angles so that every radial value has the same index a its corresponding angle
#the angles and radii are sorted so that the list of angles starts at 0
r_cmm = np.roll(r_cmm, -max_idx_theta_cmm)
r_cmm_savgol = np.roll(r_cmm_savgol, -max_idx_theta_cmm)
theta_cmm = np.roll(theta_cmm, -max_idx_theta_cmm)

#interpolate a point between CMM values that is in line with the origin and one Ansys value
interp_r_cmm = np.interp(theta_ansys, theta_cmm, r_cmm_savgol)

#create values that can plot a cirkle with a radius equal to the mean radius of the CMM values
circle = np.full(np.size(r_ansys), np.mean(interp_r_cmm))

avgdiff = np.mean(abs(r_ansys - interp_r_cmm)) #find the average difference between Ansys and CMM
diffcirc = np.mean(abs(circle - interp_r_cmm)) #find the average difference between the circle and CMM
print(avgdiff)
print(diffcirc)


plt.figure()
```

```
50 plt.plot(theta_cmm, r_cmm, color='blue') #plot noisy CMM radii
   over CMM angles
51 plt.plot(theta_cmm, r_cmm_savgol, color='red') #plot noice
   reduced CMM radii over cmm angles
52 plt.plot(theta_ansys, r_ansys, color='green') #plot Ansys radii
   over Ansys angles
53 plt.plot(theta_ansys, interp_r_cmm, color='orange') #plot
   interpolated, noice reduced CMM radii over Ansys angles
54 plt.plot(theta_ansys, circle, color='black') #plot circle over
   Ansys angles
55
56 #plot a horizontal line highlighting that the angles for the
   smallest radii in Ansys and CMM values are aligned
57 plt.axvline(theta_ansys[np.argmin(r_ansys)], color='black',
   linestyle='-.', linewidth= 0.7)
```

On rows 6, 7, 9 and 10, data gathered from simulations and CMM are imported from external files.

DEPARTMENT OF MECHANICS AND MARITIME SCIENCES
CHALMERS UNIVERSITY OF TECHNOLOGY
Gothenburg, Sweden 2026
www.chalmers.se

CHALMERS
UNIVERSITY OF TECHNOLOGY